A report submitted in partial fulfillment of the
requirements for the transfer from MPhil to PhD

SAMPLING SCHEMES FOR 2-D SIGNALS WITH FINITE RATE OF INNOVATION

by

P D Shukla

supervisor

Dr P L Dragotti

Communications and Signal Processing Group
Electrical and Electronic Engineering Department
Imperial College London
University of London

March 2005

CERTIFICATE OF APPROVAL

TRANSFER REPORT

This is to certify that the report submitted by

P D Shukla

has been approved by the Examining Committee in
partial fulfilment of the requirement for the transfer from MPhil to PhD

Examining committee:

Dr T P Stathaki

Communications and Signal Processing Group

Dr I M Jaimoukha

Control and Power Group

Electrical and Electronic Engineering Department
Imperial College London
University of London

March 2005

Scientific theories deal with concepts- not reality. Formula and theories are so formulated as to correspond in some 'useful' way to the real world. The quest for precision is analogous to the quest for certainty and both- precision and certainty are impossible to attain.

-Karl Popper

ACKNOWLEDGMENTS

First of all I acknowledge my supervisor Dr P L Dragotti for giving me an opportunity to work as a research assistant at Imperial College London on an EPSRC funded project. I am thankful to Dr Dragotti for his profound guidance, compassion, and earnest efforts to raise my aspirations. I would also like to mention that he marvels in chartering a realistic plan of work, which has been playing an important role in sustaining my enthusiasm for this involved research task.

I am grateful to Alex for my desktop troubleshooting and helping me installing necessary softwares. I am also thankful to all the familiar faces in the Communications and Signal Processing Group for their direct and indirect help in many occasions.

Although, too wonderful for words, I must not discount my wife Krupa for her spirited sacrifices in supporting my research passion.

ABSTRACT

In this report, we propose new sampling schemes for classes of 2-D signals with finite rate of innovation (FRI). In particular, we consider sets of 2-D Diracs and bilevel (and planar) polygons. As opposed to using only sinc or Gaussian kernels [23], we allow the sampling kernel to be any function that reproduces polynomials.

In the proposed sampling schemes, we exploit the polynomial approximation properties of the sampling kernels in association with other relevant techniques such as complex-moments [25], annihilating filter method [37], and directional derivatives.

Specifically, for sets of Diracs, we propose two sampling schemes: first uses local kernels and suits well to sparsely distributed Diracs, whereas the second relies on global reconstruction based on annihilating filter method, it utilizes complex-moments and is suitable for densely packed Diracs. Similarly for polygons, we propose two different reconstruction methods: the first uses a global reconstruction algorithm and complex moments, while the second is based on directional derivatives and local reconstruction algorithms.

The trade-offs among all reconstruction modalities are also summarized.

TABLE OF CONTENTS

LIST OF FIGURES

CHAPTER 1
INTRODUCTION AND CONTRIBUTION

1.1 Problem, background, and scope

We know that most natural-world phenomena are observed and analyzed through sampling, thus sampling is one of the core elements in many applications of modern science and technology. Although Shannon's sampling theory and its extensions are very powerful and have been successfully utilized for bandlimited signals, in many situations this 'bandlimited-sinc' constraint is too restrictive to abide for the available acquisition devices and processing algorithms [33].

The conventional 'bandlimited' scenario has been extended to classes of nonbandlimited signals such as uniform splines that reside in a subspace spanned by a generating function and its shifted versions [33, 3]. For a comprehensive account on the modern sampling developments, we refer to [33, 19].

Very recently, novel sampling schemes have been presented for larger classes of 1-D signals that are neither bandlimited nor reside in a subspace [37]. Such signals belong to a class of signals with a finite number of degrees of freedom (or rate of innovation) and are classified as signals with Finite Rate of Innovation (FRI). Streams of Diracs, nonuniform splines, and piecewise polynomials are examples of such signals. These novel sampling schemes feature: sinc and Gaussian sampling kernel, annihilating filter method, and perfect reconstruction using only a finite number of samples (lowpass estimates). Nevertheless, both sinc and Gaussian kernels pose difficulties in practice due to their slow decay and infinite support.

Extensions of the schemes in [37] to the 2-D case are examined in [23] and [22].

These 2-D extensions, however, protract with the sinc and Gaussian kernels.

In [11, 12, 13] it was shown that 1-D FRI signals can be sampled using a very rich class of kernels such as functions that reproduce polynomials, exponential Splines [34], and functions with rational Fourier transforms. In this report we furnish extensions of these results in 2-D; we focus on the case of 2-D kernels that can reproduce polynomials and show that sets of 2-D Diracs and polygonal images can be sampled and perfectly reconstructed using these kernels. For the polygonal case, we present two alternative schemes: one is based on complex-moments and annihilating filter method, the other on the link between finite differences and directional derivatives.

1.2 Organization of the report

In the next chapter we review the concept of FRI signals and extend it to 2-D. We focus on a 2-D generic sampling setup and to the important properties of the kernels employed in the proposed sampling schemes. In Chapter 3, a local sampling scheme for sets of 2-D Diracs is presented. In Chapter 4, we address a global scheme for sampling the bilevel polygons, inspired by the complex-moments based approach of [16, 25]. We then extend this global sampling scheme (of bilevel polygons) to sets of Diracs as an alternative to the local one presented in Chapter 3. In Chapter 5, we propose a novel directional-derivatives based sampling scheme for planar polygons. The scheme is local (involve only a corner point at a time) and holds only local complexities irrespective of the number of corner points. Finally, we conclude in Chapter 6 and outline the future work on the envisaged roadmap.

1.3 Original contribution

Chapters 3, 4, and 5 of this report present the original and individual research work. The contribution includes development of novel sampling schemes for 2-D FRI signals using a rich class of kernels that reproduce polynomials. More precisely, the contribution is enumerated as follows

1. Sampling scheme for sets of 2-D Diracs using local kernels (Proposition 1)

2. Sampling scheme for bilevel polygons and Diracs by solving a global system using complex-moments and annihilating filter method (Proposition 2 and Proposition 3)

3. Sampling scheme for planar polygons using local kernels by discovering a link between continuous directional derivatives and discrete differences over the integer lattices

CHAPTER 2
SAMPLING SIGNALS WITH FINITE RATE OF INNOVATION (FRI)

2.1 Introduction

In this chapter, first we review the concept of signals with finite rate of innovation (FRI) and then focus on its extension in 2-D. We describe two core aspects related to the sampling of 2-D FRI signals, namely, a 2-D sampling setup and classes of 2-D sampling kernels with desired properties.

2.2 Review of FRI signals

The intuitive way to introduce signals with finite rate of innovation is to think them as finite complexity signals having a parametric representation with a finite number of parameters (degrees of freedom).

More precisely, consider a signal of the form [37]

$$g(t) = \sum_{n\in\mathbb{Z}} \sum_{k=0}^{K} \lambda_{n,k}\, f_k\left(t - t_n\right) \tag{2.1}$$

where the set of functions $\{f_k\}, k = 0, 1, \ldots, K$ is known. It is clear that the only free parameters (degrees of freedom) in $g(t)$ are the time instants t_n and the coefficients $\lambda_{n,k}$.

It is therefore natural to introduce a counting function $C_g(t_a, t_b)$ that counts the number of free parameters in $g(t)$ over an interval $\tau = [t_a, t_b]$. The rate of innovation of $g(t)$ is then defined as [37]

$$\rho = \lim_{\tau \to \infty} \frac{1}{\tau} C_g \left(-\frac{\tau}{2}, \frac{\tau}{2} \right) \tag{2.2}$$

Definition 1. (Vetterli, Marziliano, Blu [37]) *A signal with a finite rate of innovation is a signal whose parametric representation is given in (2.1) and with a finite ρ as defined in (2.2).*

Notice that shift-invariant signals, including bandlimited real signals are included in Definition 1. For instance, if we call $f_m > 0$ the maximum frequency in a bandlimited real signal, then $\rho = 2f_m$. Therefore, one possible interpretation is that it is possible to sample bandlimited signals because they have finite rate of innovation. In general for FRI signals, the number of degrees of freedom can be related directly to the minimum sampling density ρ or to the minimum number of samples that allow perfect reconstruction.

In some cases it is more convenient to consider a local rate of innovation with respect to a moving window of size τ. The local rate of innovation at time t is thus given by [37]

$$\rho_\tau(t) = \frac{1}{\tau} C_g \left(t - \frac{\tau}{2}, t + \frac{\tau}{2} \right). \tag{2.3}$$

Clearly $\rho_\tau(t)$ tends to ρ as $\tau \to \infty$.

2.3 FRI signals in 2-D

The notion of FRI can be easily extended in 2-D for a signal

$$g(x, y) = \sum_{j \in \mathbb{Z}} \sum_{k \in \mathbb{Z}} \sum_{n=0}^{N} \lambda_{j,k,n} \, f_n \left(x - x_j, y - y_k \right) \tag{2.4}$$

with $\rho_{xy} = \rho_x \rho_y = \lim_{\tau_x, \tau_y \to \infty} \frac{1}{\tau_x \tau_y} C_g \left(-\frac{\tau_x}{2}, \frac{\tau_x}{2} \right) C_g \left(-\frac{\tau_y}{2}, \frac{\tau_y}{2} \right)$, where x_j and y_k are arbitrary shifts in x and y directions respectively. For example [23], when $f_n(x, y) = \delta_{xy}(x, y)$

and both $x_j - x_{j-1}$ and $y_k - y_{k-1}$ are i.i.d. random variables with exponential density, then $g(x, y)$ describes a separable 2-D Poisson process. A set of 2-D Diracs is one particular realization of a 2-D Poisson process. Other examples of 2-F FRI signals include simple lines, polygonal images, and planar parametric curves.

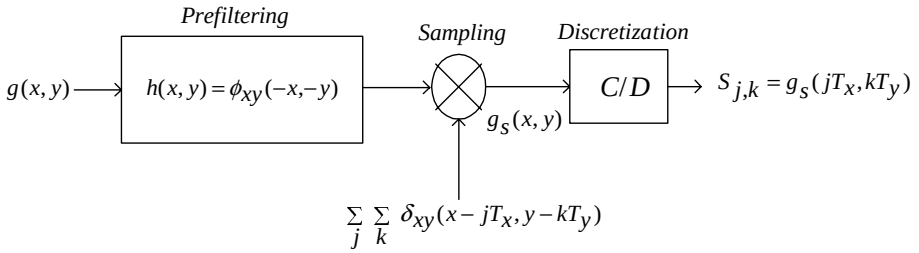

Figure 2.1: A generic 2-D sampling setup

2.4 Sampling setup in 2-D

It is customary to filter a given signal before being (uniformly) sampled. We consider a 2-D generic sampling setup, where a continuous 2-D FRI signal $g(x, y)$ is prefiltered with a smoothing (sampling) kernel $\varphi_{xy}(x, y)$. The filtered version $g(x, y) * \varphi(-x, -y)$ is sampled uniformly to obtain a set of samples $S_{j,k}$ given by

$$S_{j,k} = \langle g(x, y), \varphi_{xy}(x/T_x - j, y/T_y - k) \rangle \tag{2.5}$$

where $x, y \in \mathbb{R}$, $j, k \in \mathbb{Z}$, and $T_x, T_y \in \mathbb{R}^+$ are the sampling intervals along x and y directions respectively. Notice that Figure 2.1 depicts a model typical of many commonly used acquisition devices and processing algorithms [23].

2.5 Sampling kernels and their properties

It is always desirable to have a freedom in selecting or designing a sampling kernel $\varphi_{xy}(x, y)$ of choice. However, in practice, the kernel results from the physical properties of the acquisition device or processing algorithms and cannot be modified. Obviously, the classical 'bandlimited-sinc' sampling strategy of Shannon is too restrictive in many real-life situations, as it relies on infinite support and a slow decaying kernel (i.e. ideal low-pass filter). Therefore it is more valuable to develop sampling schemes that support a wide range of kernels which are more attainable.

It was shown in [13] that the general requirement of kernel is to be of compact support and satisfy Strang and Fix conditions [30]. Also the kernels that reproduce exponentials (e.g. E-Splines [34]), or have rational transfer functions are included in the classes of kernels suitable for sampling FRI signals.

Although, all these kernels are equally valid, in the present context we consider only a class of kernels that reproduce polynomials. To be more precise, our sampling kernel $\varphi_{xy}(x, y)$ is given by the tensor product of two 1-D functions $\varphi(t), t \in \mathbb{R}$ that can reproduce polynomials. We further assume that $\varphi_{xy}(x, y)$ is of compact support $L_x \times L_y$. The sampling kernel $\varphi_{xy}(x, y)$ then follows the property of partition of unity as given by (see Figure 2.2 (a))

$$\sum_{j=-\infty}^{\infty} \sum_{k=-\infty}^{\infty} \varphi_{xy}(x - j, y - k) = 1, \tag{2.6}$$

and the polynomial approximation as given by (see also Figure 2.2 (b) and (c))

$$\begin{aligned} \sum_{j=-\infty}^{\infty} \sum_{k=-\infty}^{\infty} C^x_{\gamma,j}\, \varphi_{xy}(x - j, y - k) &= x^\gamma \\ \sum_{j=-\infty}^{\infty} \sum_{k=-\infty}^{\infty} C^y_{\gamma,k}\, \varphi_{xy}(x - j, y - k) &= y^\gamma, \end{aligned} \tag{2.7}$$

where $\gamma = \{0, 1, \ldots, \Gamma - 1\}$ specify numbers of degrees of polynomials that the sampling kernel $\varphi_{xy}(x, y)$ can reproduce. The coefficients $C^x_{\gamma,j}$ and $C^y_{\gamma,k}$ are kernel dependent weights along x and y directions respectively.

For example, by using a B-Spline of order one, the partition of unity is illustrated in Figure 2.2 (a). The reproduction of polynomial of degree one along x axis is shown in part (b), while the reproduction of polynomial of degree one along y axis is shown in part (c).

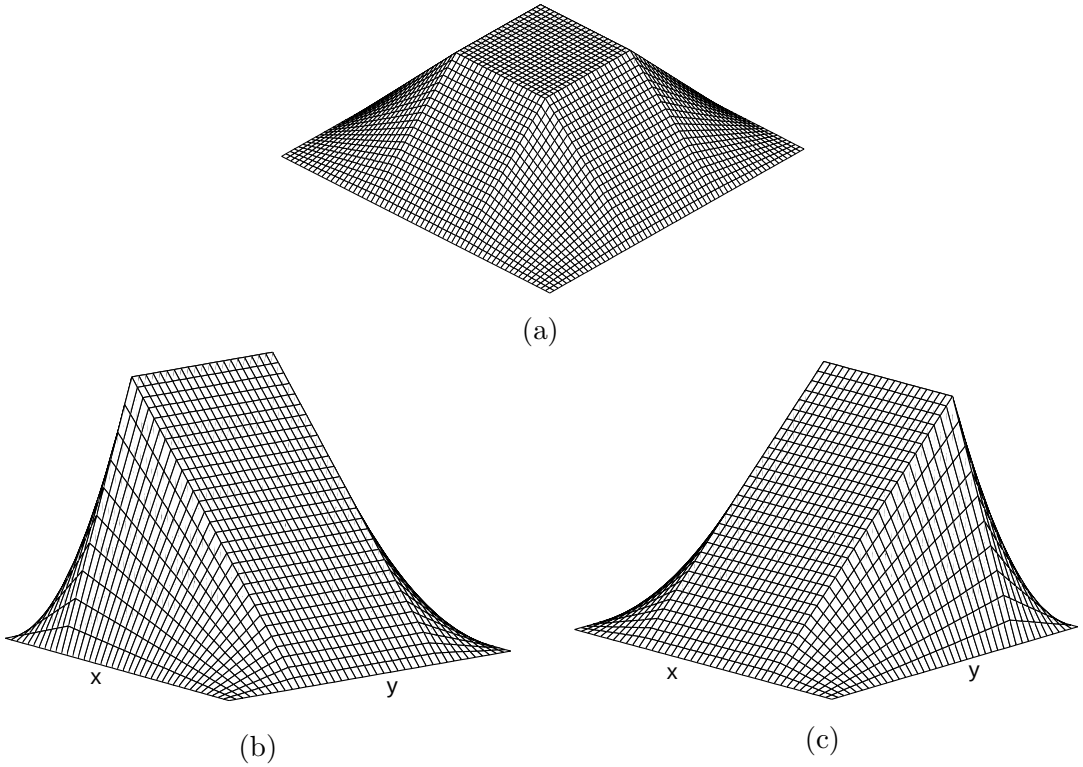

(a) (b) (c)

Figure 2.2: For example, by using a B-Spline of order 1, we have (a) Partition of unity, (b) Reproduction of polynomial of degree 1 along x axis, and (c) Reproduction of polynomial of degree 1 along y axis.

With reference to sampling and reconstructing kernels and their subspaces, it is

important to note that if the sampling kernel $\varphi_{xy}(x, y)$ is orthogonal basis then the coefficients $C^x_{\gamma,j}$, and $C^y_{\gamma,k}$ are given by

$$\begin{aligned} C^x_{\gamma,j} &= \langle x^\gamma, \varphi_{xy}(x/T_x - j, y/T_y - k)\rangle \\ C^y_{\gamma,k} &= \langle y^\gamma, \varphi_{xy}(x/T_x - j, y/T_y - k)\rangle \end{aligned} \tag{2.8}$$

while for biorthogonal basis the coefficients are given by

$$\begin{aligned} C^x_{\gamma,j} &= \langle x^\gamma, \tilde{\varphi}_{xy}(x/T_x - j, y/T_y - k)\rangle \\ C^y_{\gamma,k} &= \langle y^\gamma, \tilde{\varphi}_{xy}(x/T_x - j, y/T_y - k)\rangle \end{aligned} \tag{2.9}$$

where $\tilde{\varphi}_{xy}(x, y)$ is the dual of original kernel $\varphi_{xy}(x, y)$.

For biorthogonal bases, dual kernel plays a pivotal role in perfect reconstruction. For more details we refer to [36, 31, 6].

Notice that orthogonal Daubechies scaling functions [6] and biorthogonal B-Splines [32], among many other scaling functions, satisfy the above properties and therefore, are valid sampling kernels. Simple forms of these kernels in 2-D are shown in Figure 2.3.

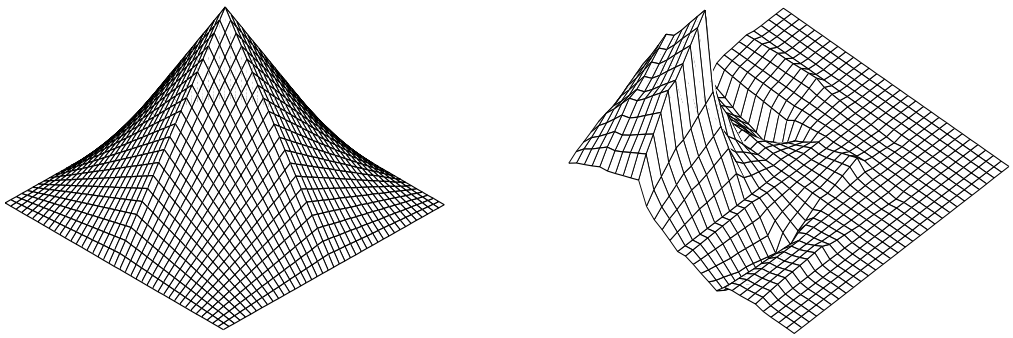

(a) (b)

Figure 2.3: (a) B-Spline of order one, (b) Daubechies scaling function using a 4-tap filter.

CHAPTER 3
SETS OF 2-D DIRACS

3.1 Introducton

In this chapter, we consider sets of 2-D Diracs as FRI signals. We will show that it is possible to sample and reconstruct sets of Diracs using local kernels that reproduce polynomials. Explicit reconstruction equations are derived and a sampling theorem is presented.

3.2 Signal model

We begin with a simple class of FRI signals, that is, a set of 2-D Diracs $g(x,y) = \sum_{j\in\mathbb{Z}} \sum_{k\in\mathbb{Z}} a_{j,k}\, \delta_{xy}\,(x - x_j, y - y_k)$, where $a, x, y \in \mathbb{R}$. Signal $g(x,y)$ is illustrated in Figure 3.1. Each Dirac can be parameterized by an amplitude and a position (in terms of two Cartesian coordinates x and y), and thus has a finite number of degrees of freedom (or rate of innovation) which equals three.

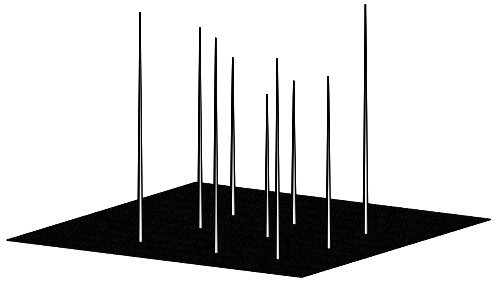

Figure 3.1: A set of 2-D Diracs

3.3 Sampling and reconstruction scheme

Assume that there is at most one Dirac in an area of size $L_xT_x \times L_yT_y$, and that the sampling kernel $\varphi_{xy}(x, y)$ can reproduce polynomials of degrees zeros and one. With the backdrop from [11], we are sure that only $L_x \times L_y$ inner products (samples) overlap in any given region of size $L_xT_x \times L_yT_y$ that encloses a unique Dirac $a_{p,q}\delta_{xy}(x-x_p, y-y_q), p, q \in \mathbb{Z}$.

Literally, for any arbitrary region enclosing a unique Dirac, equation (2.6) demonstrates the fact that an algebraic sum of shifted and overlapping kernels is constant and equals to unity (see Figure 2.2 (a)). Whereas, equation (2.7) reveals that the weighted sums of the same kernels produce 2-D unit-slope linear functions passing through the origin and in the directions governed by the weighting coefficients $C^x_{1,j}$ and $C^y_{1,k}$ (see Figures 2.2 (b) and (c)). In support of above argument, we have an analytical formulation as:

$$\begin{aligned}
\sum_{j=1}^{L_x}\sum_{k=1}^{L_y} S_{j,k} &= \left\langle a_{p,q}\delta_{xy}(x-x_p, y-y_q), \sum_{j=1}^{L_x}\sum_{k=1}^{L_y}\phi_{xy}(x-j, y-k)\right\rangle \\
&= \int_{-\infty}^{\infty} a_{p,q}\delta_{xy}(x-x_p, y-y_q)\left(\sum_{j=1}^{L_x}\sum_{k=1}^{L_y}\phi_{xy}(x-j, y-k)\right)\mathrm{d}x\,\mathrm{d}y \\
&= a_{p,q}\sum_{j=1}^{L_x}\sum_{k=1}^{L_y}\phi_{xy}(x_p-j, y_q-k) \\
&= a_{p,q} \qquad \text{(following equation (2.6))}
\end{aligned} \tag{3.1}$$

and

$$\sum_{j=1}^{L_x}\sum_{k=1}^{L_y} C^x_{1,j}S_{j,k} = \left\langle a_{p,q}\delta_{xy}(x-x_p, y-y_q), \sum_{j=1}^{L_x}\sum_{k=1}^{L_y} C^x_{1,j}\phi_{xy}(x-j, y-k)\right\rangle$$

$$
\begin{aligned}
&= \int_{-\infty}^{\infty} a_{p,q}\delta_{xy}(x-x_p, y-y_q)\left(\sum_{j=1}^{L_x}\sum_{k=1}^{L_y} C_{1,j}^{x}\phi_{xy}(x-j, y-k)\right)\mathrm{d}x\,\mathrm{d}y \\
&= a_{p,q}\sum_{j=1}^{L_x}\sum_{k=1}^{L_y} C_{1,j}^{x}\phi_{xy}(x_p-j, y_q-k) \\
&= a_{p,q}x_p \qquad \text{(following equation (2.7))} \qquad (3.2)
\end{aligned}
$$

Similarly, it is apparent to arrive at $\sum_{j=1}^{L_x}\sum_{k=1}^{L_y} C_{1,k}^{y} S_{j,k} = a_{p,q}y_q$ based on above derivation.

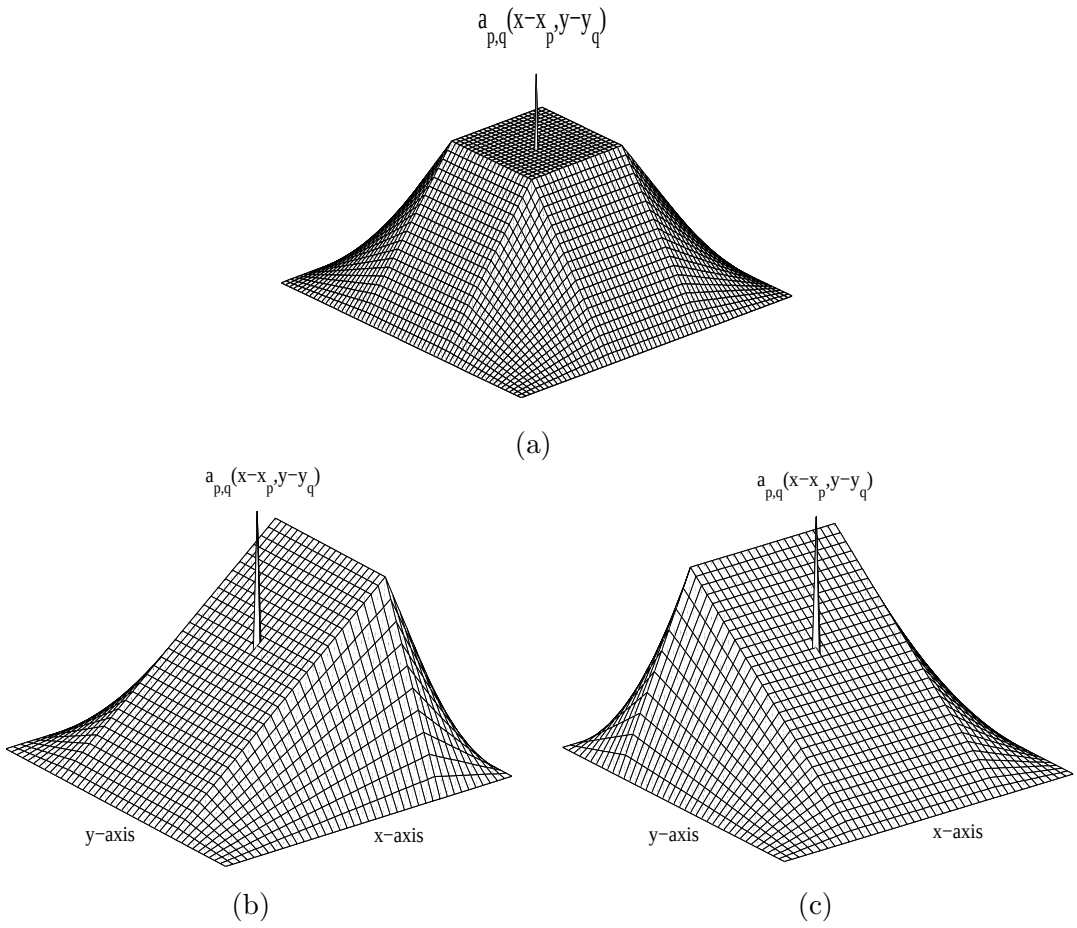

Figure 3.2: Sampling of a 2-D Dirac: (a) Partition of unity responsible for the determination of amplitude $a_{p,q}$, (b) Reproduction of polynomial of degree 1 along x direction responsible for the determination of coordinate x_p, and (c) Reproduction of polynomial of degree 1 along y direction responsible for the determination of coordinate y_q.

Therefore, the amplitude $a_{p,q}$ of a given Dirac (Figure 3.2) is reconstructed using

$$a_{p,q} = \sum_{j=1}^{L_x} \sum_{k=1}^{L_y} S_{j,k} \tag{3.3}$$

and the position (x_p, y_q) is reconstructed using

$$\begin{aligned} x_p &= \left(\sum_{j=1}^{L_x} \sum_{k=1}^{L_y} C_{1,j}^{x} S_{j,k} \right) \Big/ a_{p,q} \\ y_q &= \left(\sum_{j=1}^{L_x} \sum_{k=1}^{L_y} C_{1,k}^{y} S_{j,k} \right) \Big/ a_{p,q} \end{aligned} \tag{3.4}$$

where the coefficients $C_{1,j}^{x}$ and $C_{1,k}^{y}$ are identified from equation (2.7).

Hence, a sampling scheme for 2-D Diracs follows

Proposition 1. *Given a sampling kernel $\varphi_{xy}(x, y)$ that can reproduce polynomials of degree zero and one along both Cartesian axis x and y and of compact support $L_x \times L_y$, a set of finite amplitude 2-D Diracs $g(x, y) = \sum_{j \in \mathbb{Z}} \sum_{k \in \mathbb{Z}} a_{j,k}\, \delta_{xy}(x - x_j, y - y_k)$ is uniquely determined from its samples defined by $S_{j,k} = \langle g(x, y), \varphi_{xy}(x/T_x - j, y/T_y - k) \rangle$ if and only if there is at most one Dirac in any distinct rectangular area of size $L_x T_x \times L_y T_y$.*

CHAPTER 4
BILEVEL POLYGONS AND DIRACS: USING COMPLEX MOMENTS

4.1 Introduction

In this chapter, we consider sampling of bilevel polygons and sets of Diracs. In deriving novel sampling schemes for these signals, we use techniques such as complex-moments [16, 25] and annihilating filter [37]. We open the chapter reviewing these important techniques, and then using these techniques, we present a sampling perspective to the reconstruction of bilevel polygons and sets of Diracs.

4.2 Background

Since years, mathematicians and applied scientists have been studying the relationship between shape and moments [27, 16]. The moments of a region are the integrals of the powers of the independent variables over that region. The close relationship between shape and moments finds its application in many diverse fields such as computed tomography, geophysical inversion, and thermal imaging [16]. For example, in tomography, the X-rays compute the moments of the available object in form of line integrals (or Radon transform projections) and from these moments (or projections) the available object is characterized. Similarly, in other applications, the moment measurements avail better information to characterize an object otherwise unspecified.

Among other variants, complex (or harmonic) moments potentially provide enough information to allow complete or partial reconstruction of unknown polygonal shapes viewed as the closed regions in the complex Cartesian plane [7, 8, 29, 25, 16].

4.3 Complex-moments for polygonal shapes

Definition 2. *The n^{th} simple complex moment of a given function $g(x, y)$ over a complex Cartesian plane $z = x + iy$ in the closure $\mathcal{O}$ is given by [15]:*

$$m_n^{sc} = \int\int_{\mathcal{O}} g(x, y) z^n \, dx \, dy. \tag{4.1}$$

4.3.1 Early contributions

Earlier, Davis [8] showed that any triangular region in the complex plane is uniquely determined by its complex moments up to order 3. This results was presented based on an alternate Motzkin-Schoenberg (MS) formula which is described as follows.

Let $g(x, y)$ denote a polygon with three corner points (vertices) z_1, z_2, and z_3 in the complex plane. If A is the area of $g(x, y)$ and $h(z)$ is any analytic function in the closure $\mathcal{O}$ of $g(x, y)$, then the Motzkin-Schoenberg (MS) formula [7, 8] states that

$$\int\int_{\mathcal{O}} g(x, y) h^{''}(z) \, dx \, dy = 2A \, \det(U1)/\det(U2) \tag{4.2}$$

where

$$U1 = \begin{bmatrix} 1 & 1 & 1 \\ z_1 & z_2 & z_3 \\ h(z_1) & h(z_2) & h(z_3) \end{bmatrix} \quad \text{and} \quad U2 = \begin{bmatrix} 1 & 1 & 1 \\ z_1 & z_2 & z_3 \\ z_1^2 & z_2^2 & z_3^2 \end{bmatrix}$$

Davis [7] also generalized the MS formula for polygons with $N > 3$ corner points. It was shown that the value of the integral of the second derivative of any analytic function $h(z)$ in the closure $\mathcal{O}$ of a polygonal region $g(x, y)$ in the complex plane depends only on the values of $h(z)$ at the corner points z_i of the polygonal region. The original result is highlighted as follows [7, 25].

Theorem 1. [Davis 1964] *Let $z_1, z_2, \ldots, z_N$ designate the corner points of a polygon $g(x, y)$ in the closure $\mathcal{O}$. Then, we can find constants $\rho_1, \rho_2, \ldots, \rho_N$ depending on $z_1, z_2, \ldots, z_N$ (and the way they are connected) but independent of h, such that for all h analytic in $\mathcal{O}$*

$$\int\int_{\mathcal{O}} g(x,y)\, h''(z)\, dx\, dy = \sum_{i=1}^{N} \rho_i h(z_i). \tag{4.3}$$

If $r \geq N$ and $z_{N+1}, \ldots, z_r$ are additional points distinct from $z_1, z_2, \ldots, z_N$, and if there are constants $b_1, b_2, \ldots, b_r$ that depend only on $z_1, z_2, \ldots, z_r$ such that

$$\int\int_{\mathcal{O}} h''(z)\, dx\, dy = \sum_{i=1}^{r} b_i h(z_i) \tag{4.4}$$

for all h analytic in the closure $\mathcal{O}$, then

$$\begin{aligned} b_i &= \rho_i, \quad 1 \leq i \leq N \\ b_i &= 0, \quad N+1 \leq i \leq r. \end{aligned}$$

4.3.2 Modern applications and key connection

Recently, the problem of accurate determination of the N corner points (of polygonal shapes) form a finite number of its moments is extended with better numerical stability [17, 18]. In [16], the corner point recovery is further extended by assuming perturbed (noisy) complex moments. The estimation theory based formulation of [16] , in principle, resembles many diverse application models such as i) identifying autoregressive system using its output; ii) decomposing a signal built as a linear mixture of complex exponentials; and iii) estimating the direction of arrival (DOA) in array processing.

In fact, the modern revival of Davis's theorem and its applications can be traced back to the results of Milanfar et al. in [25]. They extended the Davis's theorem by

carefully analyzing following observations.

1. The coefficients $\{\rho_i\}$ in equation (4.3) are determined from the corner points $\{z_i\}$ of the given polygon using

$$\begin{aligned} \rho_i &= \frac{\sqrt{-1}}{2}\Big(\frac{z_{i-1}^* - z_i^*}{z_{i-1} - z_i} - \frac{z_i^* - z_{i+1}^*}{z_i - z_{i+1}}\Big) \\ &= \frac{2A_i}{(z_i - z_{i+1})(z_i - z_{i-1})}, \quad i = 0, 1, \ldots, N. \end{aligned} \tag{4.5}$$

   where z^* is the complex conjugate of z. A_i is the signed area of the triangle formed by the vertices z_{i-1}, z_i, and z_{i+1} such that

$$A_i = \frac{\sqrt{-1}}{4} \det \begin{bmatrix} z_{i-1} & z_{i-1}^* & 1 \\ z_i & z_i^* & 1 \\ z_{i+1} & z_{i+1}^* & 1 \end{bmatrix}.$$

2. No $\{\rho_i\}$ is zero unless the corresponding A_i is zero. However, the polygon is assumed to be simply connected and nondegenerate, all A_i are nonzero.

3. It is important to note that the equation (4.5) depends explicitly only on the corner points and their simple and cyclical order of connection such that the modulo operation $z_i = z_{i+N}$ holds. Therefore, the corresponding $\{\rho_i\}$ are essentially unique for a given polygon if it is assumed to be convex.

4. Equation (4.3) is a minimal representation of $h''(z)$ in the closure $\mathcal{O}$ in terms of discrete values of $h(z)$. The continuous integral depends only on the values of $h(z)$ at the corner points $\{z_i\}$ and their order, the values of h at other points over the complex plane have no significance. Additionally, since each $\{\rho_i\}$ is nonzero, the

expression (4.3) for any arbitrary analytic $h(z)$ cannot be reduced to an alternative form with fewer $\{\rho_i\}$.

Assume a closed region of a simply connected, convex, and nondegenerate polygon in the closure $\mathcal{O}$ over the complex plane $z = x + \sqrt{-1}\, y$. Let $g(x, y)$ be a bilevel indicator function representing the polygon in such a way that it takes the value '1' inside the polygon and the value '0' outside. Furthermore, as a special case, consider an analytic function $h(z) = z^n$ over the complex plane, by applying Davis's theorem, it is possible to show that [25]

$$\begin{aligned}
\sum_{i=1}^{N} \rho_i \, z_i^n &= \int\int_{\mathcal{O}} g(x,y)\, h^{''}(z)\, dx\, dy \\
&= \int\int_{\mathcal{O}} g(x,y)(z^n)^{''}\, dx\, dy \\
&= n(n-1) \int\int_{\mathcal{O}} g(x,y) z^{n-2}\, dx\, dy \\
&= n(n-1)\, m_{n-2}^{sc} \\
&= \tau_n, \quad \forall n \geq 2
\end{aligned} \tag{4.6}$$

where m_{n-2}^{sc} represents simple complex moments of the polygon $g(x, y)$ from (4.1), while $\tau_n = n(n-1)\, m_{n-2}^{sc}$, $n \geq 2$ denotes weighted complex moments, and by definition $\tau_0 = \tau_1 = 0$. Note that the coefficients $\{\rho_i\}$ are determined from equation (4.5).

Above expression holds a direct relationship between the corner points z_i and a finite number of complex moments τ_n. As such for every value of n, τ_n can be uniquely determined by evaluating the function $h(z)$ at N discrete points z_i. Whereas, in practice, the positions z_is are derived from a finite number ($\geq N$) of moments τ_ns using Prony's method [25]. (However, this becomes an estimation problem if the moments are perturbed [16]). The positions z_is are sufficient to uniquely determine the original bilevel polygon $g(x, y)$ following the assumption of its being nondegenerate, simply connected,

and convex [25].

Note that the annihilating filter method [37] is a potential algorithmic variant of the Prony's method to determine the corner points z_is from τ_ns, and is discussed in the next section.

In summary of above discussion, a key connection that is relevant to our sampling perspective is described as follows:

Theorem 2. [Milanfar et al.] *For a given nondegenerate, simply connected, convex polygon in the complex Cartesian plane, all of its N corner points are uniquely determined by its weighted complex moments τ_n up to order $2N-1$.*

4.4 Annihilating filter method

The annihilating filter method is well known in error-correction coding and spectral analysis [37]. In particular, in second application, often the weights ρ_i and locations u_i of the spectral components are required to be accurately determined from the observed signal $\tau[n]$ which is composed of linear combinations of exponentials such that $\tau[n] = \sum_{i=0}^{N-1} \rho_i \, u_i^n$, where $\rho_i \in \mathbb{R}, u_i \in \mathbb{C}, n \in \mathbb{N}$. Very recently, this method has been successfully utilized for sampling FRI signals, more accurately, in determining weights ρ_i and locations u_i for the streams of Diracs [37].

The annihilating filter method consists of two steps:

1. Designing a filter $A[l]$ that annihilates signal $\tau[n]$ such that $A[n] * \tau[n] = 0, \ \forall n \in N$.

2. Determining the locations u_i and weights ρ_i using the coefficients of filter $A[n]$ and the available signal $\tau[n]$.

Given the important role played by this method for reconstruction of FRI signals [37], and its immediate relevance in the following section, we briefly discuss its core formulation. For in-depth treatment, we recommend [37, 28].

4.4.1 Designing filter $A[n]$

Consider a signal

$$\tau[n] = \sum_{i=0}^{N-1} \rho_i \, u_i^n, \quad \rho_i \in \mathbb{R}, u_i \in \mathbb{C}, n \in \mathbb{N}, \tag{4.7}$$

and a filter $A[l]$, $l = 0, 1, \ldots, N$ with z-transform

$$A(z) = \sum_{l=0}^{N} A[l] \, z^{-1} = \prod_{i=0}^{N-1} (1 - u_i \, z^{-1}). \tag{4.8}$$

It then follows that

$$\begin{aligned} A[n] * \tau[n] &= \sum_{l=0}^{N} A[l] \, \tau[n-l] && (4.9)\\ &= \sum_{l=0}^{N} \sum_{i=0}^{N-1} \rho_i \, A[l] \, u_i^{n-l} \\ &= \sum_{i=0}^{N-1} \rho_i \underbrace{\Big(\sum_{l=0}^{N} A[l] \, u_i^{-l} \Big)}_{\text{is 0 for } z=u_i \text{ from (4.8)}} u_i^n \\ &= 0. && (4.10) \end{aligned}$$

Thus, $A[n]$ annihilates $\tau[n]$. In practice, the coefficients $A[l]$ are obtained by solving a linear system of equations characterized by $A[n] * \tau[n] = \sum_{l=0}^{N} A[l] \, \tau[n-l] = 0$. Following the fact that $A[0] = 1$, the same system in Yule-Walker form using N independent equations with $2N-1$ observations of $\tau[n]$ follows

$$\begin{bmatrix} \tau[N-1] & \tau[N-2] & \cdots & \tau[0] \\ \tau[N] & \tau[N-1] & \cdots & \tau[1] \\ \vdots & \vdots & \ddots & \vdots \\ \tau[2N-2] & \tau[2N-3] & \cdots & \tau[N-1] \end{bmatrix} \begin{bmatrix} A[1] \\ A[2] \\ \vdots \\ A[N] \end{bmatrix} = - \begin{bmatrix} \tau[N] \\ \tau[N+1] \\ \vdots \\ \tau[2N-1] \end{bmatrix}. \tag{4.11}$$

4.4.2 Determining locations u_i and weights ρ_i

The coefficients $A[n]$ of annihilating filter are determined using Yule-Walker system of (4.11), and from equation (4.8) it is straightforward to see that the N roots of filter

$A(z)$ are exactly the locations u_i.

Once the locations u_i are known, the weights ρ_i are determined by solving equations (4.7) as follows

$$\begin{bmatrix} 1 & 1 & \cdots & 1 \\ u_0 & u_1 & \cdots & u_{N-1} \\ \vdots & \vdots & \ddots & \vdots \\ u_0^{N-1} & u_1^{N-1} & \cdots & u_{N-1}^{N-1} \end{bmatrix} \begin{bmatrix} \rho_0 \\ \rho_1 \\ \vdots \\ \rho_{N-1} \end{bmatrix} = \begin{bmatrix} \tau[0] \\ \tau[1] \\ \vdots \\ \tau[N-1] \end{bmatrix}. \tag{4.12}$$

This Vandermonde system yields unique solution for the weights ρ_i, given that all locations u_i are distinct.

4.5 A sampling perspective using complex moments

With a clear background and sufficient knowledge of the techniques such as complex moments and annihilating filter method, we are now ready to propose our sampling schemes for bilevel polygons and sets of Diracs.

Let us recall our sampling setup as outlined in Section 2.4: We consider any 2-D sampling kernel $\varphi_{xy}(x, y)$ that satisfies partition of unity (2.6) and polynomial approximation (2.7) along both Cartesian axis x and y. Furthermore, for a given 2-D signal $g(x, y)$, the output samples $S_{j,k}$ are given by

$$S_{j,k} = \langle g(x, y), \varphi_{xy}(x/T_x - j, y/T_y - k) \rangle. \tag{4.13}$$

4.5.1 Bilevel polygons

Consider a simply connected, nondegenerate, and convex bilevel polygon $g(x, y)$ with N corner points and such that inside the polygons is '1' and outside is '0'. Also we have a sampling kernel $\varphi_{xy}(x, y)$ that reproduces polynomials at least up to degree

$\gamma = 2N - 1$ along both x and y directions.

Let us consider 2-D Cartesian plane xy as a complex plane z such that all N corner points $z_i = x_i + \sqrt{-1}\, y_i, \quad i = 1, 2, \ldots, N$ of $g(x, y)$ are enclosed within the closure $\mathcal{O}$. Furthermore, consistent with the definition of simple complex moments m_n^{sc}, select an analytic function $h(z) = z^n,\ n \in \mathbb{N}$. Therefore, using the formulation (4.6) of Milanfar et al., we have

$$\tau_n = \sum_{i=1}^{N} \rho_i \, z_i^n = \int_{\mathcal{O}} g(x, y)(z^n)'' \, dz = n(n-1) \int \int_{\mathcal{O}} z^{n-2} \, dx \, dy \tag{4.14}$$

since $g(x, y)$ is '1' within the closure $\mathcal{O}$ and '0' outside.

Complex moments from samples $S_{j,k}$:

It is obvious to notice that with the sampling, we cease to have direct access to the original polygon $g(x, y)$, instead we have access to the samples $S_{j,k}$. However, it is remarkable to note that the polynomial approximation property of sampling kernel allows us to link the complex moments τ_n with the complex sums of the products of samples $S_{j,k}$ and the coefficients $C_{\gamma,j}^x$ and $C_{\gamma,k}^y$.

For instance, we have

$$\begin{aligned} \tau_3 &= \sum_{i=1}^{N} \rho_i \, z_i^3 \\ &= 6 \int_{\mathcal{O}} z \, dz \\ &= 6 \int \int_{\mathcal{O}} (x + \sqrt{-1}\, y) \, dx \, dy \\ &= 6 \sum_j \sum_k (C_{1,j}^x + \sqrt{-1}\, C_{1,k}^y) \, S_{j,k}. \end{aligned} \tag{4.15}$$

Similarly, we can obtain any other moment τ_n for $n \in \mathbb{N}$. In particular, we require at least $2N - 1$ moments with $n = \gamma + 2$, $\gamma = 0, 1, \ldots, 2N - 1$, consistent with the theorem of Milanfar et al. as mentioned before on Page 19.

Determining corner points by designing $A(z)$ ***using*** τ_n***:***

It is straightforward to see that all the derived moments τ_n based on (4.15) consists linear combinations of exponentials z_i^n. Therefore, it is possible to retrieve the corner points z_i using annihilating filter method as discussed in Section 4.4. Notice that in this polygonal case, the weights ρ_i are complex and dependent on the corner points z_i. However, bilevel polygon is completely characterized by its corner points z_i.

Once we have at least $2N-1$ moments τ_n, we design an annihilating filter $A[l]$, $l = 0, 1, \ldots, N$ from τ_n using the Yule-Walker system of (4.11). The N complex roots of the filter $A(z)$ give the positions $z_i = x_i + \sqrt{-1}\, y_i$ of all the N corner points on a complex Cartesian plane. Assumption of nondegenerate, simply connected, and convex polygon guarantees a unique reconstruction.

Thus a sampling perspective to the reconstruction of bilevel polygon follows

Proposition 2. *Given a sampling kernel* $\varphi_{xy}(x, y)$*, a simply connected and convex bilevel polygon* $g(x, y)$ *with at most* N *corner points is uniquely determined by its samples* $S_{j,k} = \langle g(x, y), \varphi_{xy}(x/T_x - j, y/T_y - k)\rangle$*, provided that* $\varphi_{xy}(x, y)$ *can reproduce polynomial up to degree* $2N-1$ *along both the Cartesian axis* x *and* y*.*

4.5.2 Sets of Diracs

Now imagine a case where, instead of a bilevel polygon, signal $g(x, y)$ consists of a set of N 2-D Diracs such that

$$g(x, y) = \sum_{i=1}^{N} a_i \delta_{xy}(x - x_i, y - y_i), \quad a, x, y \in \mathbb{R}. \tag{4.16}$$

Where we assume that the set of N Diracs may be arbitrarily enclosed in a small region in the closure $\mathcal{O}$ over the complex Cartesian plane xy such that the positions of all N

Diracs are uniquely identified by $z_i = x_i + \sqrt{-1}\, y_i,\ i = 1, 2, \ldots, N$.

Notice that here we relax the earlier assumption of only one Dirac in the area of $L_xT_x \times L_yT_y$ (Recall the local reconstruction scheme for Diracs given in Chapter 3), where $L_x \times L_y$ denotes the support of 2-D sampling kernel $\varphi_{xy}(x, y)$, and T_x, T_y are the uniform sampling intervals along x and y directions.

However, consistent with the polygonal case, we consider the kernel $\varphi_{xy}(x, y)$ that can at least reproduce polynomials of degrees $\gamma = 0, 1, \ldots, 2N - 1$ along both x and y directions. Also assume that there are at most N Diracs in any distinct area of size $NL_xT_x \times NL_yT_y$. Justification of this assumption is in the line with its 1-D formulation and is rigorously discussed in [13]. Since we have assumed that there are up to N Diracs in an arbitrary small region, we need to consider the global reconstruction of at most N Diracs at the same time rather than a local one that considers only one Dirac at a time (Chapter 3).

In the following discussion, we show that it is straight forward to extend the complex-moments based sampling scheme of bilevel polygon to the set of N Diracs. Again we employ annihilating filter method in solving a system of $2N$ polynomial equations.

Agreeing with the polynomial reproduction property of the sampling kernel, consider the analytic function $h(z) = z^n = (x + \sqrt{-1}\, y)^n,\ n \in \mathbb{N}$ in the closure $\mathcal{O}$ that encloses a set of N Diracs $g(z) = g(x, y)$. Then from the formulation (4.6) of Milanfar et al., we can find the complex-moments τ_n as given by

$$\begin{aligned}
\tau_n &= \int\int_{\mathcal{O}} g(z)\, h(z)\, dz \\
&= \int\int_{\mathcal{O}} g(x,y)\, z^n\, dx\, dy \\
&= \int\int_{\mathcal{O}} \sum_{i=1}^{N} a_i \delta_{xy}(x-x_i, y-y_i)\ (x+\sqrt{-1}\, y)^n\, dx\, dy \\
&= \sum_{i=1}^{N} a_i\, z_i^n, \quad n=\gamma
\end{aligned} \tag{4.17}$$

where a_i identifies amplitudes and z_i identifies positions of all N Diracs over the 2-D complex plane, and $\gamma = 0, 1, \ldots, 2N-1$.

From a sampling perspective, owing to the polynomial reproduction property of the sampling kernel, complex sums of linear combinations of samples $S_{j,k} = \langle g(x,y), \varphi_{xy}(x/T_x - j, y/T_y - k)\rangle$ and the corresponding weights $C^x_{\gamma,j}$ and $C^y_{\gamma,j}$ produce at least $2N-1$ complex-moments τ_n.

For example, when $\varphi_{xy}(x,y)$ belongs to the classes of either orthogonal Daubechies scaling functions or biorthogonal B-Splines then it follows that

$$\tau_n = \sum_{j=1}^{N}\sum_{k=1}^{N} \left(C^x_{1,j} + \sqrt{-1}\, C^y_{1,k}\right)^n\ S_{j,k} \tag{4.18}$$

where $n=\gamma$ for $\gamma = 0, 1, \ldots, 2N-1$, and $C^x_{\gamma,j} = (C^x_{1,j})^n$ and $C^y_{\gamma,k} = (C^y_{1,k})^n$.

Now equating the righthand sides of equations (4.17) and (4.18), we have

$$\sum_{i=1}^{N} a_i\, z_i^n = \sum_{j\in\mathbb{Z}}\sum_{k\in\mathbb{Z}} \left(C^x_{1,j} + \sqrt{-1}\, C^y_{1,k}\right)^n\ S_{j,k} \tag{4.19}$$

where the righthand side gives $2N-1$ simple complex moments of the signal $g(x,y)$ from its samples $S_{j,k}$ for $n=\gamma$.

Clearly in analogy with the case of bilevel polygon, it is easy to follow that equation (4.19) is solved for the weights a_i and positions z_i using the annihilating filter method.

The N roots of the annihilating filter $A(z)$ derived from the Yule-Walker system of (4.11) give exact positions. Once the positions are known, the amplitudes are obtained from the Vandermonde system of (4.12). Distinctiveness of all Diracs guarantees a unique solution.

Thus a sampling perspective to the reconstruction of Diracs follows

Proposition 3. *Given is a sampling kernel $\varphi_{xy}(x, y)$ with compact support $L_x \times L_y$. A set of finite amplitude Diracs $g(x, y) = \sum_{i\in\mathbb{Z}} a_i \delta_{xy}(x - x_i, y - y_i)$ is uniquely determined from its samples $S_{j,k} = \langle g(x, y), \varphi_{xy}(x/T_x - j, y/T_y - k)\rangle$ if and only if there are at most N Diracs in an area of size $NL_xT_x \times NL_yT_y$ and the kernel $\varphi_{xy}(x, y)$ can reproduce polynomials up to degree $2N - 1$ along both the Cartesian axis x and y.*

4.5.3 Simulation results

Now we present simulation results for two simple cases; i) a bilevel polygon with three corner points, and ii) a set of three Diracs.

Simulation result for the bilevel is illustrated in Figure 4.1. Figure 4.1 (a) shows the original bilevel polygonal image with corner points $N = 3$. We get a low resolution version of the image $g(x, y)$ by convolving it with the smoothing (sampling) kernel $\varphi_{xy}(x, y)$. This low resolution version is depicted in Figure 4.1 (b). A sampled version of $g(x, y) * \varphi_{xy}(-x, -y)$, with uniform sampling interval in both x and y direction, is shown in part (c). From these samples, using complex-moments, we can retrieve the exact locations of the corner points. The reconstructed corner points are indicated with $+$ in Figure 4.1 (a). In part (d), we show a B-Spline sampling kernel $\varphi_{xy}(x, y) = \beta^5_{xy}(x, y)$ that we have used for the simulation. The kernel reproduces polynomial up to degrees

$2N-1=5$ in both x and y directions.

In the second case, out of three Diracs, the second Dirac has one of its positional coordinates x_p and y_q shared with the first Dirac and the remaining coordinate is shared with the third one. Note that, in this type of situation one cannot retrieve the correct positions of all Diracs using separable moments [23], however it is possible with the complex-moments.

Simulation result for the set of $N=3$ Diracs is illustrated in Figure 4.2. Figure 4.2 (a) shows the input image $g(x,y)$ that consists of three Diracs. We get a low resolution version of the image $g(x,y)$ by convolving it with the smoothing (sampling) kernel $\varphi_{xy}(x,y)$. The low resolution version is depicted in Figure 4.2 (b). A sampled version of $g(x,y) * \varphi_{xy}(-x,-y)$, with uniform sampling interval in both x and y direction, is shown in part (c), notice that the only inner products (samples) that overlap Diracs are nonzero. From the set of 40×40 samples, using complex-moments, we can retrieve the exact locations of the Diracs. The reconstructed Diracs are superimposed over the set of samples $S_{j,k}$ and are shown in Figure 4.2 (c). In part (d), we show a B-Spline sampling kernel $\varphi_{xy}(x,y) = \beta^5_{xy}(x,y)$ that we have used for the simulation. The kernel reproduces polynomial up to degrees $2N-1=5$ in both x and y directions.

4.6 Summary

The complex-moments based approach provides a global solution for the reconstruction of bilevel polygons and sets of Diracs. The complexity of the solution, however, increases with the complexity of the signal g(x, y) (i.e. with the number of corner points or Diracs). Moreover, polygons with very close corner points and very closely placed Diracs pose a reconstruction challenge due to numerical instabilities in the algorithmic implementations.

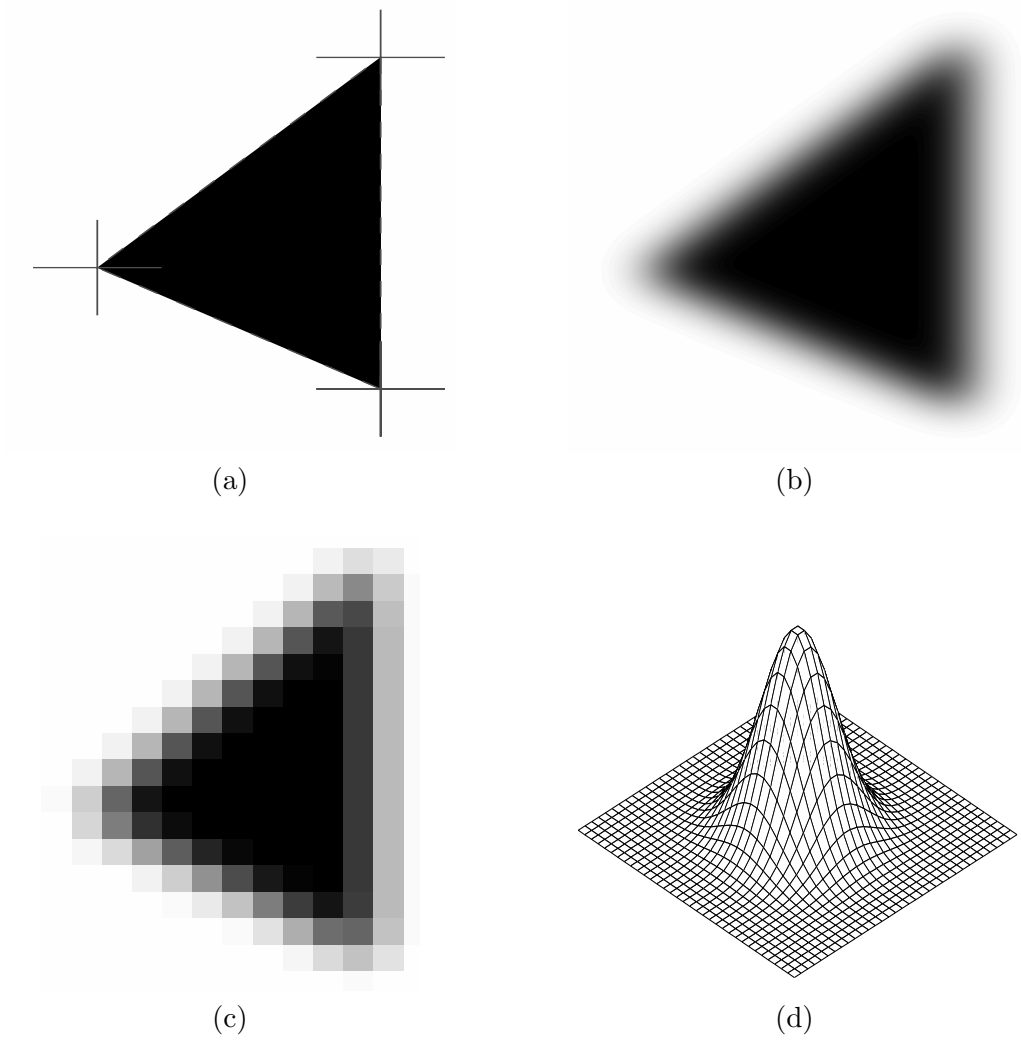

Figure 4.1: (a) An original bilevel polygon and $N = 3$ reconstructed corner points (with $+$). The input image $g(x, y)$ is of size 2971×2971 pixels. (b) The lower resolution version $g(x, y) * \varphi_{xy}(-x, -y)$ of $g(x, y)$ available due to convolution with a smoothing kernel $\varphi_{xy}(x, y)$. (c) The set of 22×22 samples obtained by uniform sampling of $g(x, y) * \varphi_{xy}(-x, -y)$. (d) The B-Spline sampling kernel $\varphi_{xy}(x, y) = \beta^5_{xy}(x, y)$ with support 661×661 pixels that can reproduce polynomials up to degree five along both x and y.

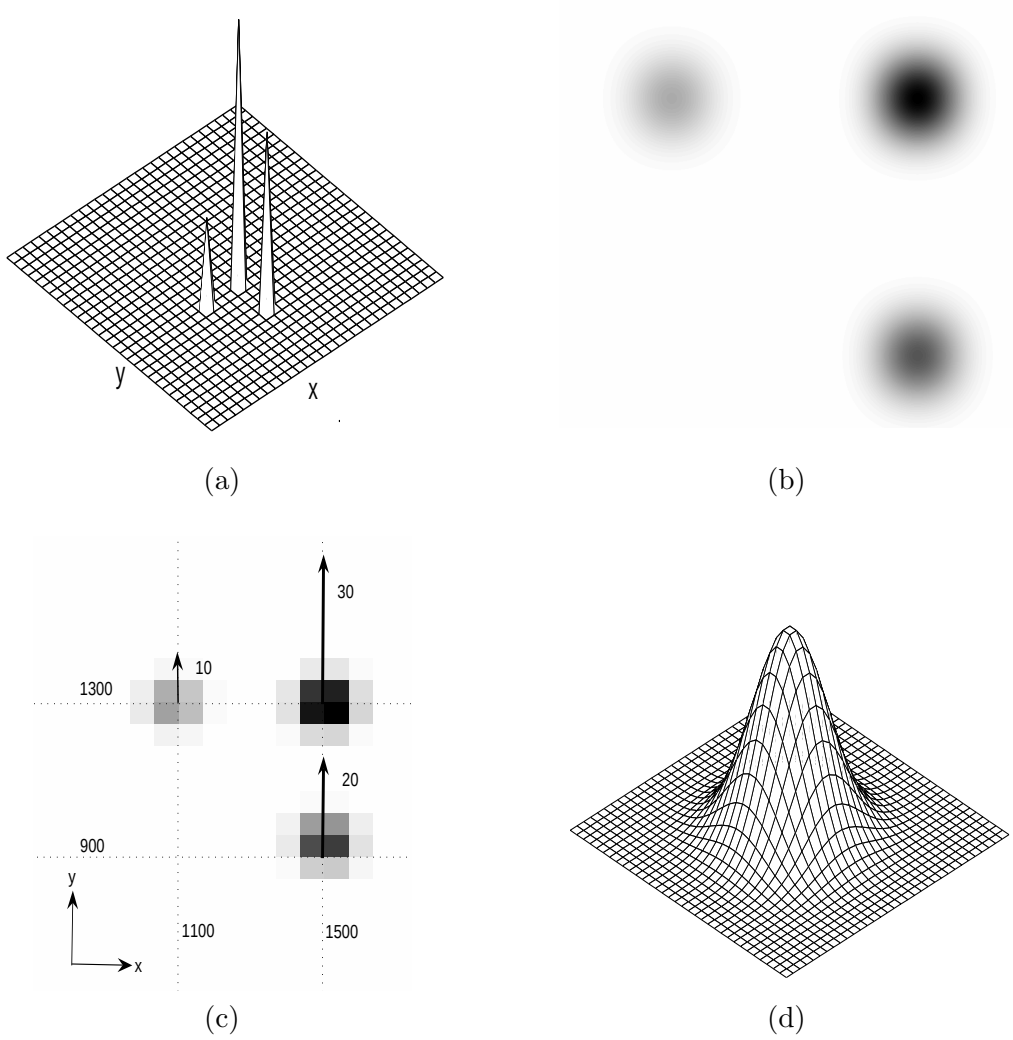

Figure 4.2: (a) An input image $g(x, y)$ with $N = 3$ Diracs. The input image $g(x, y)$ is of size 3031×3031 pixels. (b) The lower resolution version $g(x, y) * \varphi_{xy}(-x, -y)$ of $g(x, y)$ is available due to convolution with a smoothing kernel $\varphi_{xy}(x, y)$. (c) The set of 40×40 samples obtained by uniform sampling of $g(x, y) * \varphi_{xy}(-x, -y)$, however the only inner products (samples) that overlap Diracs are nonzero. The reconstructed Diracs are superimposed over the samples. (d) The B-Spline sampling kernel $\varphi_{xy}(x, y) = \beta^5_{xy}(x, y)$ with support 379×379 pixels that can reproduce polynomials up to degree five along both x and y.

CHAPTER 5
PLANAR POLYGONS: DIRECTIONAL DERIVATIVES BASED APPROACH

5.1 Introduction

In this chapter, we consider sampling of planar polygons. We discover the link between continuous directional derivatives and discrete directional differences based on the fundamentals of lattice theory. In particular, we exploit subsampling over integer lattices. We integrate the resultant 'directional' kernels in the local sampling scheme for 2-D Diracs and derive accurate reconstruction equations for the polygonal corner points.

5.2 Problem formulation

5.2.1 Continuous model

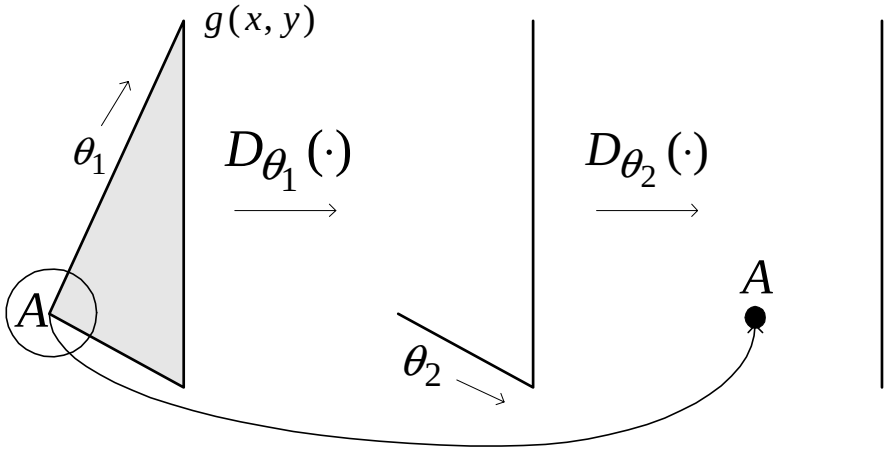

Figure 5.1: A proper combination of two successive directional derivatives $\mathcal{D}_{\theta_1}$ and $\mathcal{D}_{\theta_2}$ decomposes a corner point A into a 2-D Dirac for a given planar polygon $g(x, y)$.

Intuitively, we agree upon the fact that for an arbitrary planar polygon, two successive directional derivatives along two adjacent polygonal sides will result into a 2-D Dirac at the corner point formed by the respective sides. In supplementing this assertion, we have a simple illustration as given in Figure 5.1. In the illustration, we show a planar polygon $g(x, y)$ with $N = 3$ corner points. A proper combination of two successive directional derivatives $\mathcal{D}_{\theta_1}$ and $\mathcal{D}_{\theta_2}$ along the orientations θ_1 and θ_2 decomposes a corner point A into a 2-D Dirac.

Let us review the formal model of directional derivatives in 2-D by considering a continuous planar polygon $g(x, y)$ with N corner points. All N sides (boundaries) of the polygon are identified by the 2-D lines as given by

$$y_i = \tan(\theta_i)\, x_i + b_i, \quad i = 1, 2, \ldots, N, \quad x, y, \theta, b \in \mathbb{R} \tag{5.1}$$

where b_i are shifts (offsets) and θ_i are the orientations in Cartesian $x\,y$ plane.

Now focus onto an arbitrary corner point (e.g. point A in Figure 5.1) of the given polygon $g(x, y)$ formed by the two adjacent polygonal sides with orientations θ_1 and θ_2. A set of two successive directional derivatives $\mathcal{D}_{\theta_1}$ and $\mathcal{D}_{\theta_2}$ on $g(x, y)$ follows that [1]

$$\begin{aligned}
\mathcal{D}_{\theta_2}\left[\mathcal{D}_{\theta_1}\left[g(x,y)\right]\right] &= \mathcal{D}_{\theta_2}\left[\cos(\theta_1)\frac{\partial}{\partial x}\Big(g(x,y)\Big) + \sin(\theta_1)\frac{\partial}{\partial y}\Big(g(x,y)\Big)\right] \\
&= \cos(\theta_2)\frac{\partial}{\partial x}\left(\cos(\theta_1)\frac{\partial}{\partial x}\Big(g(x,y)\Big) + \sin(\theta_1)\frac{\partial}{\partial y}\Big(g(x,y)\Big)\right) + \\
&\quad \sin(\theta_2)\frac{\partial}{\partial y}\left(\cos(\theta_1)\frac{\partial}{\partial x}\Big(g(x,y)\Big) + \sin(\theta_1)\frac{\partial}{\partial y}\Big(g(x,y)\Big)\right) \\
&= \cos(\theta_1)\cos(\theta_2)\frac{\partial^2}{\partial x^2}\Big(g(x,y)\Big) + \sin(\theta_1+\theta_2)\frac{\partial}{\partial y}\Big(\frac{\partial}{\partial x}\Big(g(x,y)\Big)\Big) + \\
&\quad \sin(\theta_1)\sin(\theta_2)\frac{\partial^2}{\partial y^2}\Big(g(x,y)\Big).
\end{aligned} \tag{5.2}$$

Notice that the formulation (5.2) offers a generalized solution for decomposing a

planar polygon into a set of N 2-D Diracs using N independent iterations. These N Diracs are precisely located at the corresponding N corner points of a given $g(x, y)$. Notice that this formulation requires suitable combinations of $2N$ directional derivatives along the desired orientations θ_i, $i = 1, 2, \ldots, N$. It is worth to register that we will employ this formulation later in the proposed sampling scheme.

Furthermore, a thoughtful analysis of (5.2) reveals a potential link of reconstructing planar polygons in the framework of 2-D Diracs (Chapter 3).

5.2.2 Discrete challenge

In practice, we do not have direct access to the polygon $g(x, y)$ but only to the samples $S_{j,k} = \langle g(x, y), \varphi_{xy}(x/T_x - j, y/T_y - k)\rangle$, where $\varphi_{xy}(x, y)$ is the sampling kernel. For simplicity, Figure 5.2 illustrates the discretization of $g(x, y)$ with $N = 3$ corner points using the Haar scaling function (or B-Spline $\beta^0_{xy}(x, y)$ of order zero) as a sampling kernel.

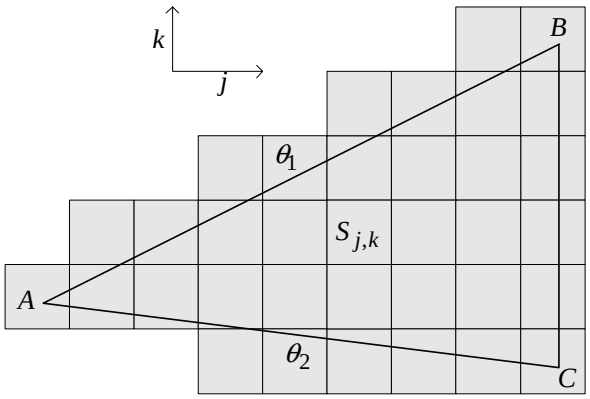

Figure 5.2: Representation of $g(x, y)$ with a finite number of samples $S_{j,k}$. For simplicity, the sampling kernel $\phi_{xy}(x, y)$ is a 2-D Haar scaling function (or a B-spline $\beta^0_{xy}(x, y)$ of order zero).

However, a discrete equivalent to the directional derivatives over $g(x, y)$ is the evaluation of directional differences over the set of samples $S_{j,k}$. The connection between the

two dwells in the lattice theory, and in particular, involves subsampling over rectangular lattices of $\mathbb{Z}^2$ (2-D integer lattices).

In the next section, we review important properties of integer lattices. Then in the subsequent section, by exploiting these properties we establish a link between directional derivatives and directional differences. Incidentally, this link is governed by the local 'directional' kernels that reproduce polynomials. Eventually employing these kernels in the framework of 2-D Dirac sampling we reconstruct the corner points from a finite number of samples $S_{j,k}$.

5.3 Lattice Theory

As we are dealing with a finite number of samples $S_{j,k}, j, k \in \mathbb{Z}$ over a uniform rectangular grid, we focus onto the 2-D integer lattices. A quick overview on the fundamentals of the lattice theory can be found in [2, 14, 21, 24, 26, 35]. For a detailed treatment we refer to [4, 5].

5.3.1 Base lattice

A full rank integer lattice Λ is a subset of points of $\mathbb{Z}^2$, which can be represented by two linear combinations of the basis vectors $\{\vec{v}_1, \vec{v}_2\}$ with integer coefficients as given by [9, 35]

$$\Lambda = \{\lambda : \lambda = n_1\vec{v}_1 + n_2\vec{v}_2\}, \quad n_i, \vec{v}_i \in \mathbb{Z},\ i = 1, 2 \tag{5.3}$$

where a row vector $\vec{v}_i = \{v_{i,1}, v_{i,2} \mid i = 1, 2\}$.

5.3.2 Sampling matrix

The resultant lattice Λ satisfying $\Lambda \subset \mathbb{Z}^2$ is the outcome of subsampling over integer lattice $\mathbb{Z}^2$. The subsampling scheme is characterized by a non-unique sampling matrix (generator matrix) V_Λ [9, 35]:

$$V_\Lambda = \begin{pmatrix} \vec{v}_1 \\ \vec{v}_2 \end{pmatrix} = \begin{pmatrix} v_{1,1} & v_{1,2} \\ v_{2,1} & v_{2,2} \end{pmatrix} \tag{5.4}$$

For example, the matrix $V_\Lambda = \begin{pmatrix} 1 & 2 \\ 2 & -1 \end{pmatrix}$ can be identified with the basis vectors $\{\vec{v_1}, \vec{v_2}\}$ as shown in Figure 5.3. The determinant of V_Λ is denoted by $\det(V_\Lambda)$, and for the mentioned case $\det(V_\Lambda) = -1 - 4 = -5$. If V_Λ is the sampling matrix for Λ, then all the possible sampling matrices of Λ (representing same sampling process) are given by UV_Λ where U is a unimodular matrix satisfying $|\det(U)| = 1$.

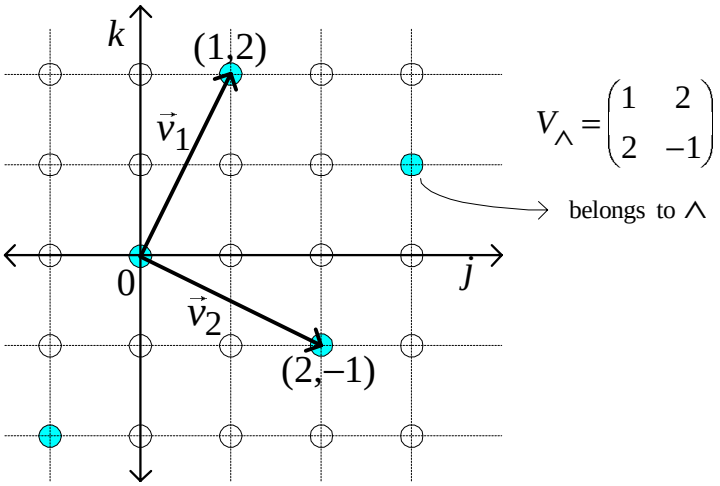

Figure 5.3: Basis vectors $\{\vec{v_1}, \vec{v_2}\}$ that determines the sampling matrix V_Λ for the base lattice Λ.

5.3.3 Cosets

For a given base lattice Λ, characterized by the sampling matrix V_Λ and its determinant $\det(V_\Lambda)$, it is possible to partition the integer lattice $\mathbb{Z}^2$ into $|\det(V_\Lambda)|$ cosets

$$\Lambda_{\sigma,i} = \Lambda + \Lambda_i^{'},\ i = 0, 1, ..., |\det(V_\Lambda)| - 1 \tag{5.5}$$

where $\Lambda_{\sigma,i}$ are the shifted versions of the base lattice Λ [9]. For example, an interleaving pattern of $|\det(V_\Lambda)|$ cosets $(\Lambda_{\sigma,i})$ of the base lattice Λ is highlighted in Figure 5.4, where the base lattice has a sampling matrix V_Λ as depicted in Figure 5.3.

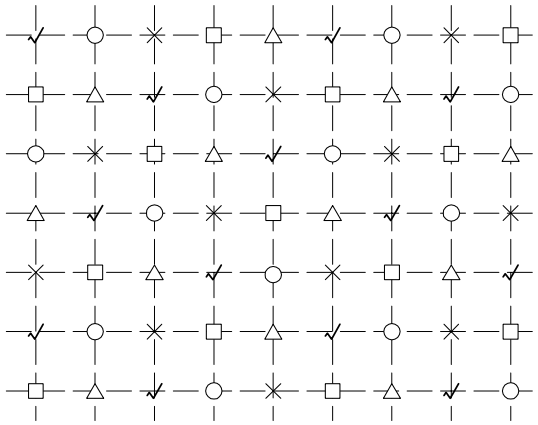

Figure 5.4: Interleaving pattern of five cosets (as marked with $\surd, \bigcirc, \times, \square, \triangle$). The original base lattice Λ is same as shown in Figure 5.3.

5.3.4 Unit cell

$\mathcal{P}_\Lambda(j,k)$ is a unit cell of the integer lattice $\Lambda \in \mathbb{Z}^2$ if it satisfies [20]:

1. $\mathcal{P}_\Lambda(j,k) \subset \mathbb{Z}^2,\ j,k \in \mathbb{Z}$,

2. $\bigcup_{(m,n)\in\Lambda} (\mathcal{P}_\Lambda(j,k) + (m,n)) = \mathbb{Z}^2$, and

3. $(\mathcal{P}_\Lambda(j,k) + (m_1,n_1)) \bigcap (\mathcal{P}_\Lambda(j,k) + (m_2,n_2)) = 0$
   for $m_1 \neq m_2$, $n_1 \neq n_2$, and m_1,n_1,m_2,$n_2 \in \Lambda$.

In other words, unit cell is a set of points of integer lattice Λ such that disjoint union of its copies shifted to all of the lattice points of Λ yield the input integer lattice $\mathbb{Z}^2$. The examples of important unit cells include parallelogram and Voronoi cell. Parallelogram is formed by two basis vectors $\{\vec{v}_1, \vec{v}_2\}$ of the lattice Λ. Voronoi cell is a set of points closer to the origin than to any other lattice point. In frequency domain, the unit cell $\mathcal{P}_\Lambda^f$ of the reciprocal lattice Λ^f is an example of Voronoi cell [21].

Determinant $\det(V_\Lambda)$ represent the area of the unit cell of the lattice Λ as well as an inverse of the sampling density.

5.3.5 Reciprocal lattice

The reciprocal lattice Λ^f is the Fourier transform of the original lattice Λ, and its points represent replicated spectra in the frequency domain. This periodicity allows the shifted copies of the unit cell $\mathcal{P}_\Lambda^f$ (frequency domain) to cover the entire spectra of Λ^f [20].

5.3.6 Subsampling effect in frequency domain

Consider I as an original integer lattice $\mathbb{Z}^2$. If the subsampled lattice Λ with the sampling matrix V_Λ follows $\Lambda(j,k) = I(V_\Lambda j, V_\Lambda k),\ j,k \in \mathbb{Z}$ then the following relation holds in the frequency domain [21]:

$$\Lambda^f(\omega_x, \omega_y) = \frac{1}{|\det(V_\Lambda)|} \sum_{j\in\mathbb{Z}} \sum_{k\in\mathbb{Z}} I^f \left(\{V_\Lambda{}^T\}^{-1} \cdot (\omega_x - j r_x, \omega_y - k r_y) \right) \tag{5.6}$$

where V_Λ^T is the transpose of the sampling matrix V_Λ, r_x, r_y are the basis vectors of the reciprocal lattice Λ^f, i.e. $r_x, r_y \in \Lambda^f$, and the vectors $\omega_x, \omega_y \in \mathbb{R}$.

Equation (5.6) suggests that a 2-D continuous signal sampled over the lattice Λ has a spectral content scaled by $\frac{1}{|\det(V_\Lambda)|}$ and is periodic over the reciprocal lattice Λ^f with the period determined by the basis vectors r_x, r_y. For a bandlimited signal, the spectral

content is confined within the unit cell (Voronoi cell) $\mathcal{P}_{\Lambda}^{f}$ formed by the reciprocal sampling matrix $(V_{\Lambda}{}^{T})^{-1}$ characterized by the basis vectors r_x, r_y [20].

5.4 Proposed sampling scheme

Consider a planar polygon $g(x, y),\ x, y \in \mathbb{R}$ with N corner points. The N sides of the polygon are described by $y_i = \tan(\theta_i)\, xi + b_i,\ i = 1, 2, \ldots, N$, where $\theta_i \in \mathbb{Q}$ represents the orientations and b_i represents offsets. Assume that the corner points are sufficiently apart (precise quantification is exposed later). Furthermore, we have access to the samples $S_{j,k} = \langle g(x, y), \varphi_{xy}(x/T_x - j, y/T_y - k)\rangle$, where the kernel $\varphi_{xy}(x, y)$ satisfies partition of unity (2.6).

Let us focus onto a set of samples $S_{j,k}$ around an arbitrary corner point of polygon $g(x, y)$ (e.g. point A in Figure 5.2) formed by the two adjacent sides, oriented along θ_1 and θ_2 respectively.

Consider the base lattice $\Lambda = \{\lambda : \lambda = n_1\vec{v}_1 + n_2\vec{v}_2\}$ with $n_i, \vec{v}_i \in \mathbb{Z}$, and $\vec{v}_i = \{v_{i,1}, v_{i,2} | i = 1, 2\}$. The base lattice is characterized by a (non-unique) sampling matrix $V_{\Lambda} = \begin{pmatrix} v_{1,1} & v_{1,2} \\ v_{2,1} & v_{2,2} \end{pmatrix}$ with its determinant defined as $\det(V_{\Lambda})$. The row vectors $\vec{v}_1$ and $\vec{v}_2$ are chosen such that $\theta_1 = \tan^{-1}\left(\frac{v_{1,2}}{v_{1,1}}\right)$, and $\theta_2 = \tan^{-1}\left(\frac{v_{2,2}}{v_{2,1}}\right)$.

5.4.1 Connecting directional differences to derivatives

Following the modus operandi as depicted in Figure 5.5, apply a pair of directional differences $\mathcal{D}_{\theta_1}$ and $\mathcal{D}_{\theta_2}$ along θ_1 and θ_2 over the two pairs of samples $S_{j,k}$ (identified by Λ). It then follows that

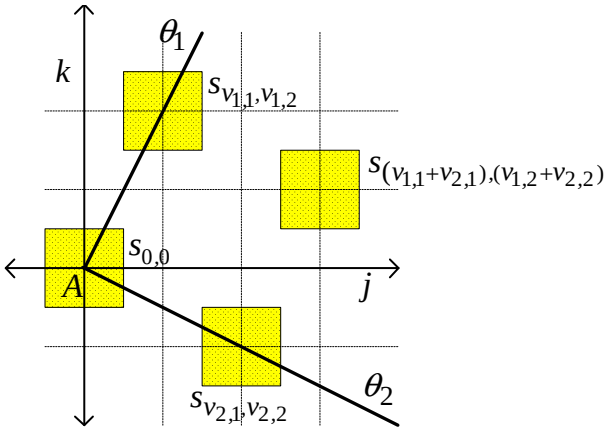

Figure 5.5: Two successive directional differences $\mathcal{D}_{\theta_1}$ and $\mathcal{D}_{\theta_2}$ evaluated along θ_1 and θ_2 over the two pairs of samples $S_{j,k}$ around an arbitrary corner point A of the planar polygon $g(x, y)$.

$$
\begin{aligned}
\mathcal{D}_{\theta_2}\left[\mathcal{D}_{\theta_1}\left[S_{j,k}\right]\right] &= \left\{S_{(v_{2,1}+v_{1,1}),(v_{2,2}+v_{1,2})} - S_{(v_{2,1}),(v_{2,2})}\right\} - \left\{S_{(v_{1,1}),(v_{1,2})} - S_{0,0}\right\} \\
&= \Big\langle g(x,y), \\
&\quad \Big\{\varphi_{xy}(x-(v_{2,1}+v_{1,1}), y-(v_{2,2}+v_{1,2})) - \varphi_{xy}(x-v_{2,1}, y-v_{2,2})\Big\} - \\
&\quad \Big\{\varphi_{xy}(x-v_{1,1}, y-v_{1,2}) - \varphi_{xy}(x-0, y-0)\Big\}\Big\rangle.
\end{aligned}
$$

Using Parseval's identity, it follows that

$$
\begin{aligned}
\mathcal{D}_{\theta_2}\left[\mathcal{D}_{\theta_1}\left[S_{j,k}\right]\right] &= \frac{1}{2\pi}\Big\langle \hat{g}(\omega_x,\omega_y), \hat{\varphi}_{xy}(\omega_x,\omega_y)\cdot\Big(\\
&\quad \Big\{e^{-j\left((v_{2,1}+v_{1,1})\omega_x+(v_{2,2}+v_{1,2})\omega_y\right)} - e^{-j\left(v_{2,1}\omega_x+v_{2,2}\omega_y\right)}\Big\} - \\
&\quad \Big\{e^{-j\left(v_{1,1}\omega_x+v_{1,2}\omega_y\right)} - 1\Big\}\Big)\Big\rangle \\
&= \frac{1}{2\pi}\Big\langle \hat{g}(\omega_x,\omega_y), \hat{\varphi}_{xy}(\omega_x,\omega_y)\cdot \\
&\quad \Big(e^{-j\left(v_{1,1}\omega_x+v_{1,2}\omega_y\right)} - 1\Big)\cdot\Big(e^{-j\left(v_{2,1}\omega_x+v_{2,2}\omega_y\right)} - 1\Big)\Big\rangle.
\end{aligned}
$$

After multiplying and dividing by the same factors, it becomes

$$\begin{aligned}\mathcal{D}_{\theta_2}\left[\mathcal{D}_{\theta_1}\left[S_{j,k}\right]\right] &= \frac{1}{2\pi}\Bigg\langle \hat{g}(\omega_x,\omega_y), \hat{\varphi}_{xy}(\omega_x,\omega_y)\cdot \\ &\quad \Big(j(v_{1,1}\omega_x + v_{1,2}\omega_y)\Big)\cdot\Big(j(v_{2,1}\omega_x + v_{2,2}\omega_y)\Big)\cdot \\ &\quad \frac{\Big(e^{-j\left(v_{1,1}\omega_x+v_{1,2}\omega_y\right)}-1\Big)\Big(e^{-j\left(v_{2,1}\omega_x+v_{2,2}\omega_y\right)}-1\Big)}{\Big(j(v_{1,1}\omega_x + v_{1,2}\omega_y)\Big)\Big(j(v_{2,1}\omega_x + v_{2,2}\omega_y)\Big)}\Bigg\rangle. \end{aligned} \tag{5.7}$$

Now recall that $\hat{\beta}_t^0(\omega) = \frac{1-e^{-j\omega\, t}}{j\omega}$ is the frequency domain representation of B-Spline of order zero. This representation can be extended in 2-D as given by

$$\begin{aligned}\hat{\beta}^0_{\theta_1}(\omega_x,\omega_y) &= \left.\frac{(1-e^{-j(v_{1,1}\omega_x+v_{1,2}\omega_y)})}{j(v_{1,1}\omega_x + v_{1,2}\omega_y)}\right|_{\theta_1=\tan^{-1}\left(\frac{v_{1,2}}{v_{1,1}}\right)} \\ \hat{\beta}^0_{\theta_2}(\omega_x,\omega_y) &= \left.\frac{(1-e^{-j(v_{2,1}\omega_x+v_{2,2}\omega_y)})}{j(v_{2,1}\omega_x + v_{2,2}\omega_y)}\right|_{\theta_2=\tan^{-1}\left(\frac{v_{2,2}}{v_{2,1}}\right)} \\ \hat{\beta}^0_{\theta_1,\theta_2}(\omega_x,\omega_y) &= \hat{\beta}^0_{\theta_1}(\omega_x,\omega_y)\cdot\hat{\beta}^0_{\theta_2}(\omega_x,\omega_y). \end{aligned} \tag{5.8}$$

where $\hat{\beta}^0_{\theta_1}$ and $\hat{\beta}^0_{\theta_2}$ are the B-Splines of order zero along orientations θ_1 and θ_2 respectively. The directional (or skewed) B-Spline $\hat{\beta}^0_{\theta_1,\theta_2}$ is depicted in Figure 5.6.

For simplicity, let

$$\hat{\xi}_{\theta_1,\theta_2}(\omega_x,\omega_y) = \hat{\beta}^0_{\theta_1,\theta_2}(\omega_x,\omega_y)\hat{\varphi}_{xy}(\omega_x,\omega_y). \tag{5.9}$$

Substituting the identities of (5.8) and (5.9) in the formulation of (5.7), we have that

$$\begin{aligned}\mathcal{D}_{\theta_2}\left[\mathcal{D}_{\theta_1}\left[S_{j,k}\right]\right] &= \frac{1}{2\pi}\Bigg\langle \hat{g}(\omega_x,\omega_y), \hat{\xi}_{\theta_1,\theta_2}(\omega_x,\omega_y)\cdot \\ &\quad (j(v_{1,1}\omega_x + v_{1,2}\omega_y))\cdot(j(v_{2,1}\omega_x + v_{2,2}\omega_y))\Bigg\rangle \\ &= \frac{1}{2\pi}\Bigg\langle \hat{g}(\omega_x,\omega_y), \hat{\xi}_{\theta_1,\theta_2}(\omega_x,\omega_y)\cdot \\ &\quad \Big\{(j\omega_x)^2 v_{1,1}\, v_{2,1} + (j\omega_x)(j\omega_y)(v_{1,1}\, v_{2,2} + v_{1,2}\, v_{2,1}) + \\ &\quad (j\omega_y)^2 v_{1,2}\, v_{2,2}\Big\}\Bigg\rangle. \end{aligned}$$

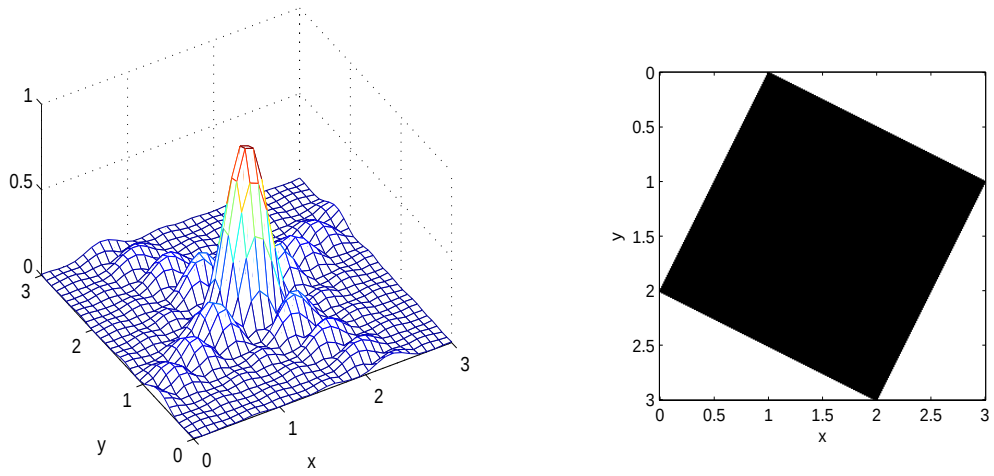

(a) $\hat{\beta}^0_{\theta_1,\theta_2}(\omega_x, \omega_y)$ (b) $\beta^0_{\theta_1,\theta_2}(x, y)$

Figure 5.6: The directional 2-D B-Spline: (a) $\beta^0_{\theta_1,\theta_2}$ in frequency domain (low resolution to highlight the sinc shape). The skewness of the sinc depends on the basis vectors $\{\vec{v}_1, \vec{v}_2\}$ that are related to the orientations θ_1 and θ_2. (b) $\beta^0_{\theta_1,\theta_2}$ in spatial domain. (In this example $\tan(\theta_1) = 2$ and $\tan(\theta_2) = -1/2$.)

Multiplying and dividing by the factor $|v_1||v_2|$, we have

$$\begin{aligned}\mathcal{D}_{\theta_2}\left[\mathcal{D}_{\theta_1}\left[S_{j,k}\right]\right] &= \frac{|v_1||v_2|}{2\pi}\Bigg\langle \hat{g}(\omega_x,\omega_y), \hat{\xi}_{\theta_1,\theta_2}(\omega_x,\omega_y)\cdot \\ &\quad \Big\{(j\omega_x)^2\frac{v_{1,1}\,v_{2,1}}{|v_1||v_2|} + (j\omega_x)(j\omega_y)\frac{(v_{1,1}\,v_{2,2}+v_{1,2}\,v_{2,1})}{|v_1||v_2|} + \\ &\quad (j\omega_y)^2\frac{v_{1,2}\,v_{2,2}}{|v_1||v_2|}\Big\}\Bigg\rangle.\end{aligned}$$

Again using the following identities in the righthand side of above equation,

$$\begin{aligned} v_{1,1} &= |v_1|\cos(\theta_1), \qquad v_{1,2} = |v_1|\sin(\theta_1) \\ v_{2,1} &= |v_2|\cos(\theta_2), \qquad v_{2,2} = |v_2|\sin(\theta_2) \\ |\det(V_\Lambda)| &= |v_{1,1}\,v_{2,2} - v_{1,2}\,v_{2,1}|, \qquad |v_1||v_2| = \frac{|\det(V_\Lambda)|}{|\sin(\theta_2-\theta_1)|}\end{aligned}$$

we have,

$$\begin{aligned}\mathcal{D}_{\theta_2}\left[\mathcal{D}_{\theta_1}\left[S_{j,k}\right]\right] &= \frac{|\det(V_\Lambda)|}{2\pi|\sin(\theta_2-\theta_1)|}\Bigg\langle \hat{g}(\omega_x,\omega_y), \hat{\xi}_{\theta_1,\theta_2}(\omega_x,\omega_y)\cdot \\ &\quad \Big\{(j\omega_x)^2\cos(\theta_1)\cos(\theta_2)+(j\omega_x)(j\omega_y)\sin(\theta_1+\theta_2)+ \\ &\quad (j\omega_y)^2\sin(\theta_1)\sin(\theta_2)\Big\}\Bigg\rangle.\end{aligned}$$

Again using Parseval's identity, we have

$$\begin{aligned}\mathcal{D}_{\theta_2}\left[\mathcal{D}_{\theta_1}\left[S_{j,k}\right]\right] &= \frac{|\det(V_\Lambda)|}{|\sin(\theta_2-\theta_1)|}\Bigg\langle g(x,y), \Big\{\cos(\theta_1)\cos(\theta_2)\frac{\partial^2}{\partial x^2}\Big(\xi_{\theta_1,\theta_2}(x,y)\Big)+ \\ &\quad \sin(\theta_1+\theta_2)\frac{\partial}{\partial y}\Big(\frac{\partial}{\partial x}\Big(\xi_{\theta_1,\theta_2}(x,y)\Big)\Big)+ \\ &\quad \sin(\theta_1)\sin(\theta_2)\frac{\partial^2}{\partial y^2}\Big(\xi_{\theta_1,\theta_2}(x,y)\Big)\Big\}\Bigg\rangle.\end{aligned}$$

Comparing the righthanded of above equation with the continuous directional derivative model of equation (5.2), it follows that

$$\begin{aligned}\mathcal{D}_{\theta_2}\left[\mathcal{D}_{\theta_1}\left[S_{j,k}\right]\right] &= \frac{|\det(V_\Lambda)|}{|\sin(\theta_2-\theta_1)|}\left\langle g(x,y), \frac{\partial}{\partial\theta_2}\Big(\frac{\partial}{\partial\theta_1}\Big(\xi_{\theta_1,\theta_2}(x,y)\Big)\Big)\right\rangle \\ &= \frac{|\det(V_\Lambda)|}{|\sin(\theta_2-\theta_1)|}\left\langle \frac{\partial}{\partial\theta_2}\Big(\frac{\partial}{\partial\theta_1}\Big(g(x,y)\Big)\Big), \xi_{\theta_1,\theta_2}(x,y)\right\rangle.\end{aligned}$$

Above equation can be presented in an equivalent form as,

$$\begin{aligned}\frac{\mathcal{D}_{\theta_2}\left[\mathcal{D}_{\theta_1}\left[S_{j,k}\right]\right]}{|\det(V_\Lambda)|} &= \left\langle \frac{\partial}{\partial\theta_2}\Big(\frac{\partial}{\partial\theta_1}\Big(g(x,y)\Big)\Big), \frac{1}{|\sin(\theta_2-\theta_1)|}\xi_{\theta_1,\theta_2}(x,y)\right\rangle \\ &= \left\langle \frac{\partial}{\partial\theta_2}\Big(\frac{\partial}{\partial\theta_1}\Big(g(x,y)\Big)\Big), \zeta_{\theta_1,\theta_2}(x,y)\right\rangle \qquad (5.10)\end{aligned}$$

where $\zeta_{\theta_1,\theta_2}(x,y) = \frac{\xi_{\theta_1,\theta_2}(x,y)}{|\sin(\theta_2-\theta_1)|} = \frac{\beta^0_{\theta_1,\theta_2}(x,y)*\varphi_{xy}(x,y)}{|\sin(\theta_2-\theta_1)|}$ is a modified sampling kernel.

5.4.2 Directional kernels

The resultant kernel $\zeta_{\theta_1,\theta_2}(x,y)$, a modified form of the original sampling kernel $\varphi_{xy}(x,y)$, is the result of the directional differences over the set of samples $S_{j,k} \subset \mathbb{Z}^2$. In other words, it is an outcome related to the discrete processing (subsampling) over the cosets of the base lattice Λ.

Because the structural properties of this modified kernel depend on the orientations θ_1 and θ_2, we denote this modified kernel as a 'directional' kernel. The kernel $\zeta_{\theta_1,\theta_2}(x,y)$ is local and with compact support $(|v_{1,1}|+|v_{1,2}|+L_x)\times(|v_{2,1}|+|v_{2,2}|+L_y)$. The presence of amplitude scaling factors $\frac{1}{|\det(V_\Lambda)|}$ and $\frac{1}{|\sin(\theta_2-\theta_1)|}$ in equation (5.10) is due to subsampling over lattices and to structural properties of the directional kernel. For example, given a corner point bounded by θ_1 and θ_2, and the original sampling kernel $\varphi_{xy}(x,y)$ is a Haar scaling function, the directional kernel $\zeta_{\theta_1,\theta_2}(x,y)$ is shown in Figure 5.7. It is important to note that for each distinct corner point, there exists an independent directional kernel $\zeta_{\theta_1,\theta_2}(x,y)$.

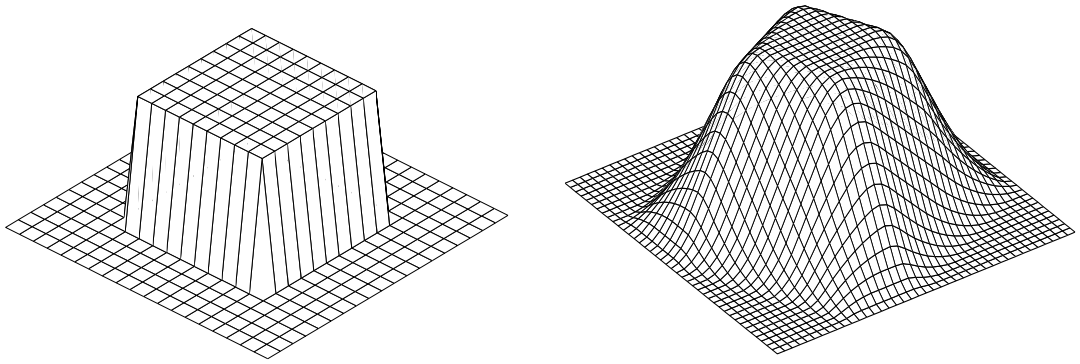

(a) (b)

Figure 5.7: For example, (a) $\varphi_{xy}(x,y)$ is a Haar scaling function with support 1×1, (b) Modified kernel $\zeta_{\theta_1,\theta_2}(x,y)$ with support 4×4 for an arbitrary corner point of the polygon formed by the two sides with orientations $\tan(\theta_1)=2/1$ and $\tan(\theta_2)=-1/2$.

5.4.3 Local reconstruction

Note that in equation (5.10), the term $\frac{\partial}{\partial\theta_2}\Big(\frac{\partial}{\partial\theta_1}\Big(g(x,y)\Big)\Big)$ represents a Dirac at a given corner point, and the support of the directional kernel is $(|v_{1,1}| + |v_{1,2}| + L_x) \times (|v_{2,1}| + |v_{2,2}| + L_y)$.

Therefore, if all N corner points of a given polygon $g(x,y)$ are arranged in such a manner that there exists a unique corner point in the area of overlapping inner products of its associated directional kernel $\zeta_{\theta_1,\theta_2}(x,y)$, then it is possible to mimic the local reconstruction scheme of 2-D Diracs as given in Chapter 3.

Given a valid sampling kernel $\varphi_{xy}(x,y)$, the directional kernel $\zeta_{\theta_1,\theta_2}(x,y)$ always satisfies partition of unity (2.6) and reproduces polynomials of degree one along both x and y directions (2.7). These properties of the modified kernel $\zeta_{\theta_1,\theta_2}(x,y)$ enable us to determine the amplitude $a_{p,q}$ and coordinate positions x_p, y_q of the resultant 2-D Dirac at a given corner point from the set of samples $S_{j,k}$. We need only a finite number of samples, i.e. $(|v_{1,1}| + |v_{2,1}| + L_x) \times (|v_{1,2}| + |v_{2,2}| + L_y)$ in the vicinity of the corner point. Hence the local reconstruction scheme of (3.3) and (3.4) generalizes as follows

$$a_{p,q} = \frac{\sum_j \sum_k \mathcal{D}_{\theta_2}\left[\mathcal{D}_{\theta_1}\left[S_{j,k}\right]\right]}{|\det(V_\Lambda)|} \tag{5.11}$$

$$x_p = \frac{\sum_j \sum_k C_{\gamma,j}\, \mathcal{D}_{\theta_2}\left[\mathcal{D}_{\theta_1}\left[S_{j,k}\right]\right]}{a_{p,q}\,|\det(V_\Lambda)|} \qquad y_q = \frac{\sum_j \sum_k C_{\gamma,k}\, \mathcal{D}_{\theta_2}\left[\mathcal{D}_{\theta_1}\left[S_{j,k}\right]\right]}{a_{p,q}\,|\det(V_\Lambda)|} \tag{5.12}$$

where for $\gamma = 0, 1$, the sets of weighting coefficients $C^x_{\gamma,j}$ and $C^y_{\gamma,k}$ associated with the kernel $\zeta_{\theta_1,\theta_2}(x,y)$ satisfy equation (2.7).

Clearly, $a_{p,q}$ gives an amplitude of $g(x,y)$, whereas the coordinate pair (x_p, y_q) gives a position of the given corner point.

5.4.4 Functional algorithm

In practice, the input image $g(x, y)$ is an arbitrary planar polygon with N corner points, such that the orientations of its sides are not known in advance. However, the polygonal reconstruction scheme based on directional derivatives is realized by the following 4-step algorithm.

1. For an input polygonal image $g(x, y)$ with N corner points, obtain a set of samples $S_{j,k} = \langle g(x, y), \varphi_{xy}(x/T_x - j, y/T_y - k)\rangle$ using a kernel $\varphi_{xy}(x, y)$.

2. By a finite number of iterations along the valid orientations (where $\tan(\theta) \in \mathbb{Q}$) and over the set of $S_{j,k}$, identify N correct pairs of directional differences.

3. Applying these pairs on $S_{j,k}$, decompose the polygonal region into N 2-D Diracs such that they are precisely located at the positions of their corresponding corner points.

4. Now for each Dirac, using the local reconstruction scheme of (5.11) and (5.12), determine the amplitude $a_{p,q}$ and the position (x_p, y_q).

5.5 Summary

The directional derivatives based sampling scheme is suitable for resolving planar polygons with varying amplitudes and with a large range of orientations ($\tan(\theta) \in \mathbb{Q}$) of their sides using only a finite number of samples. Yet, there must be at most one corner point in the area that equals the support of its associated kernel $\zeta_{\theta_1,\theta_2}(x, y)$. The advantage is that this scheme has a local reconstruction complexity irrespective of the number of corner points in a given polygon.

CHAPTER 6
CONCLUSION AND FUTURE WORK

6.1 Conclusion

In this report we have proposed several sampling schemes for the classes of 2-D nonbandlimited signals. In particular, we showed that sets of Diracs and (bilevel or planar) polygons can be reconstructed from their samples by employing sampling kernels that reproduce polynomials. Combining the tools like annihilating filters, complex-moments and directional derivatives, we provide local and global sampling choices with varying degrees of complexity.

This research has resulted into a submission of the paper:

- P. Shukla and P. L. Dragotti, "Sampling scheme for 2-D signals with finite rate of innovation using kernels that reproduce polynomials," IEEE International Conference on Image Processing (ICIP), September 2005, Genova, Italy, Submitted.

6.2 Future work

We plan to extend our work on generalizing the sampling schemes and explore their cross-fertilization with the potential extensions of wavelet footprints in 2-D [10]. In order to achieve these objectives, we have chartered the following roadmap.

From March 2005 - October 2005

- Improving algorithmic implementations for polygons considering more number of corner points and more orientations.
- Exploring a different class of kernels, namely, exponential splines (E-Splines).
- Extending the sampling schemes in higher dimensions. For instance, by using the notion of complex numbers in 4-D (quaternion).
- Considering more intricate cases. For example, piecewise polynomials inside the polygons, and planar shapes with piecewise polynomial boundaries.

We plan to submit a paper for the IEEE Transactions on Image Processing by the end of summer 2005 based on the results of above proposed work in conjunction with the results of submitted conference paper.

From November 2005 - June 2006

- Studying the notion of wavelet footprints and then extending them in 2-D.
- Integrating the proposed sampling schemes with the footprints in 2-D.
- Investigating the sampling situations when the signals are perturbed with the noise.
- Developing resolution enhancement algorithms for satellite images.

APPENDIX 1
CAMERA READY PAPER FOR ICIP2005

REFERENCES

[1] T. Aach, I. Stuke, C. Mota, and E. Barth. Estimation of multiple local orientations in image signals. In *Proceedings of ICASSP-2004*, pages III 553–556, Montreal, Canada, May 17–21 2004. IEEE.

[2] P. Agniel. Subsampling models and anti-alias filters for 3-D automultiscopic displays. Master's thesis, Boston University, February 2004.

[3] A. Aldroubi and K. Grochenig. Non–uniform sampling in shift–invariant spaces. *SIAM Review*, 43:585–620, 2001.

[4] J. W. Cassels. *An Introduction to Geometry of Numbers*. Springer-Verlag, Berlin, 1971.

[5] J. H. Conway and N. J. A. Sloane. *Sphere Packing, Lattices and Groups*. Springer-Verlag, 1998.

[6] I. Daubechies. *Ten Lectures on Wavelets*. Society for Industrial and Applied Mathematics, Philadelphia, PA, 1992.

[7] P. J. Davis. Triangle formulas in the complex plane. *Mathematics of Computation*, 18:569–577, 1964.

[8] P. J. Davis. Plane regions determined by complex moments. *Journal of Approximation Theory*, 19:148–153, 1977.

[9] P. Dragotti, V. Velisavljevic, M. Vetterli, and B. Beferull-Lozano. Discrete directional wavelet bases and frames for image compression and denoising. *Proc. of SPIE Conference on Wavelet Applications in Signal and Image Processing, X wavelets, San Diego, USA*, August 2003. Invited paper.

[10] P. L. Dragotti and M. Vetterli. Wavelet footprints: Theory, algorithms and applications. *IEEE Transactions on Signal Processing*, 51(5):1306–1322, May 2003.

[11] P. L. Dragotti and M. Vetterli. Wavelet and footprint sampling of signals with a finite rate of innovation. In *Proceedings of IEEE International Conference on Acoustics, Speech and Signal Processing (ICASSP)*, Montreal, Canada, May 2004.

[12] P. L. Dragotti, M. Vetterli, and T. Blu. Exact sampling results for signals with finite rate of innovation using Strang-Fix conditions and local kernels. In *Proceedings of IEEE International Conference on Acoustics, Speech and Signal Processing (ICASSP)*, Philadelphia, USA, March 2005.

[13] P. L. Dragotti, M. Vetterli, and T. Blu. On sampling and resolution enhancement of signals with finite rate of innovation. *IEEE Transactions on Signal Processing*, in preparation.

[14] E. Dubois. The sampling and reconstruction of time-varying imagery with application in video systems. *Proceedings of IEEE*, 73(4):502–522, April 1985.

[15] S. Durocher. Graph-theoretic and geometric algorithms associated with moment-based polygon reconstruction. Master's thesis, Computer Science Dept., University of Brithish Columbia, Vancouver, Canada, 1999.

[16] M. Elad, P. Milanfar, and G. H. Golub. Shape from moments- an estimation theory perspective. *IEEE Transactions on Signal Processing*, 52(7):1814–1829, July 2004.

[17] G. H. Golub, P. Milanfar, and J. Varah. A stable numerical method for inverting shape from moments. *SIAM Journal of Scientific Computation*, 21(4):1222–1243, December 1999.

[18] P. Gustafsson, B. Milanfar and M. Putinar. Reconstructing planar domains from their moments. *Inverse Problems*, 16(4):1053–1070, August 2000.

[19] A. J. Jerry. The Shannon sampling theorem—its various extensions and applications: A tutorial review. *Proceedings of the IEEE*, 65:1565–1596, November 1977.

[20] J. Konrad and P. Agniel. Subsampling models and anti-alias filters for 3-D automultiscopic displays. *IEEE Transactions on Image Processing*, June 2004. Submitted, E-print.

[21] J. Kovačević and M. Vetterli. Nonseparable multidimensional perfect reconstruction filter banks and wavelet bases for $\mathcal{R}^n$. *IEEE Transactions on Information Theory*, 38(2):533–555, March 1992.

[22] I. Maravić and M. Vetterli. A sampling theorem for the radon transform of finite complexity objects. In *Proceedings of IEEE International Conference on Acoustics, Speech and Signal Processing (ICASSP)*, Orlando, Florida, USA, May 2002.

[23] I. Maravić and M. Vetterli. Exact smapling results for some classes of parametric nonbandlimited 2-D signals. *IEEE Transactions on Signal Processing*, 52(1):175–189, January 2004.

[24] R. Marks II. Multidimensional-signal sample dependency at Nyquist densities. *Journal of Optical Society of America*, 3(2):268–273, February 1986.

[25] P. Milanfar, G. Verghese, W. Karl, and A. Willsky. Reconstructing polygons from moments with connections to array processing. *IEEE Transactions on Signal Processing*, 43:432–443, February 1995.

[26] D. Petersen and D. Middleton. Sampling and reconstruction of wave-number-limited functions in n-dimensional euclidean space. *Inf. Control*, 5:279–323, 1962.

[27] J. Shohat and J. Tamarkin. The problem of moments. Mathematical Surveys, volume 1, Waverly Press, Baltimore, 1943.

[28] P. Stoica and R. Moses. *Introduction to Sprectal Analysis*. Prentice-Hall, Englewood Cliffs,NJ, 2000.

[29] V. Strakhov and M. Brodsky. On the uniqueness of the inverse log-arithmic potential problem. *SIAM Journal of Applied Mathematics*, 46:324–344, 1986.

[30] G. Strang and Fix. G. Fourier analysis of the finite element variational method. *Constructive Aspects of Functional Analysis, Rome, Italy*, pages 796–830, 1971.

[31] G. Strang and T. Nguyen. *Wavelets and Filterbanks*. Wellesley-Cambridge Press, Boston, 1996.

[32] M. Unser. Splines - a perfect fit for signal and image processing. *IEEE Signal Processing Magazine*, 16:22–38, November 1999.

[33] M. Unser. Sampling—50 Years after Shannon. *Proceedings of the IEEE*, 88(4):569–587, April 2000.

[34] M. Unser and T. Blu. Cardinal exponential splines: Part I- theory and filtering algorithms. *IEEE Transactions on Signal Processing*, in press.

[35] V. Velisavljevic, B. Beferull-Lozano, M. Vetterli, and P. Dragotti. Discrete multi-directional wavelet bases. In *Proceedings of ICASSP-2003*, Barcelona, Spain, September 2003. IEEE.

[36] M. Vetterli and J. Kovacevic. *Wavelets and Subband Coding*. Prentice-Hall, Englewood Cliffs, NJ, 1995.

[37] M. Vetterli, P. Marziliano, and T. Blu. Sampling signals with finite rate of innovation. *IEEE Transactions on Signal Processing*, 50(6):1417–1428, June 2002.